NTNU

Norwegian University of
Science and Technology

Waveform Design for Software Defined Multifunctional RF Systems

Anders Åsheim

Master of Science in Electronics

Submission date: July 2017

Supervisor: Torbjørn Ekman, IES

Co-supervisor: Jonas Moen, FFI
Thomas Thoresen, FFI
Kimmo Kansanen, IES

Norwegian University of Science and Technology
Department of Electronic Systems

Problem Statement

With the recent development of more powerful Software Defined Radios (SDR), combining RF functions on the same hardware is an interesting research topic. Emphasis is given to the combination of simultaneous communication, radar, and electronic warfare capabilities. Design of a suitable waveform that performs well for all functions is required.

In this project, different properties of a multifunctional RF system implemented on an SDR platform needs to be analyzed. This includes design, implementation, and evaluation of waveforms suitable for such a system. Different properties of the system need to be theoretically analyzed, simulated, and evaluated according to suitable performance metrics.

Abstract

In this thesis, a study of multifunctional radio frequency (RF) systems implementing radar, communication, and electronic warfare (EW) is presented. Development of low cost and highly adaptable software defined radios (SDRs) enables implementation of RF systems where waveforms are digitally synthesized. An SDR capable of simultaneously performing multiple RF functions (radar, communication, and EW), has the potential to replace multiple specialized systems. In such multifunctional systems, it is necessary to optimize the waveform for all RF functions. The impact waveform design optimization has on the different RF functions needs to be quantified.

Waveform design for common-off-the-shelf (COTS) SDRs are further analyzed in this thesis. Identifying degrees of freedom with respect to spread spectrum waveform design enables simultaneous multifunction. Performance requirements for the RF functions, and the effects of waveform design choices are formally analyzed. MATLAB tools to generate, analyze and simulate multifunctional waveforms have been implemented. This allows the design space to be analyzed and simulated. *Linear frequency modulated (LFM)*, *phase coded* and *pseudo-noise* waveforms have been exploited to spread sequences of information symbols. Based on application areas, the generated waveforms have been investigated and simulated.

Key characteristics of different waveforms have been identified. LFM has high dynamic range. Results show significant reduction in dynamic range when used as a spreading sequence. Complex Gaussian noise has strong EW protection capabilities with a high instantaneous bandwidth. Using noise as a spreading sequence give promising simulation results. However, it requires high resolution in a real-world radar and communication receiver. Phase coded waveforms are proven effective for radar, communication, and EW. It has the same bandwidth as comparable Gaussian noise, but with a constant amplitude allowing simpler hardware.

In addition, a multifunctional radio frequency system (MRFS) prototype has been implemented and demonstrated on an SDR. An anti-drone scenario was chosen to demonstrate this prototype. A waveform was optimized to meet scenario specific parameters. The waveform was implemented based on results from simulation. Experimental results confirm that the phase coded waveform can simultaneously detect drones, synchronize communication, and jam a IEEE 802.11 Wi-Fi link. Experiments using a 1 W radar implementation successfully detected the drone at 70 m. At the same time, it was transmitting modulated symbols at a bit rate of 1.5 Mbps. 25 MHz bandwidth gives a range resolution of 6 m. The waveform was also capable of jamming the Wi-Fi link with a jamming-to-signal strength of 3 dB. This demonstrates the feasibility of simultaneous multifunction on COTS SDRs.

Sammendrag

I denne oppgaven presenteres en studie av multifunksjonelle radio frekvens (RF) systemer som kombinerer radar, kommunikasjon, og elektronisk krigføring (EK). Utviklingen av lav-kost programvare definerte radioer (SDR) muliggjør implementering av RF-systemer hvor bølgeformene er syntetisert digitalt. En SDR som er kapabel til å simultant utføre flere RF funksjoner (radar, kommunikasjon og EK), har et potensiale til å erstatte flere spesialiserte systemer. I slike multifunksjonelle systemer vil det være nødvendig å optimalisere bølgeformen for alle RF funksjonene. En slik optimalisering krever at virkningene av bølgeformdesign må bli identifisert.

Bølgeformdesign for hyllevare SDR er videre analysert i oppgaven. Identifisering av frihetsgrader for spredt spektrum bølgeformdesign muliggjør simultan multifunksjon. Ytelseskriterier for RF-funksjonene, og effekten av bølgeformdesign er analysert. Det er blitt implementert MATLAB-verktøy for å generere, analysere og simulere multifunksjonelle bølgeformer. Dette muliggjør analyse og simulering av løsningsrommet. Lineær frekvensmodulert (LFM), fase-kodet, og pseudo-støy bølgeformer har vært utnyttet til å spre sekvenser av informasjonssymboler. De genererte bølgeformene er blitt studert og simulert basert på applikasjonsområder.

Viktige egenskaper til forskjellige bølgeformer har blitt identifisert. LFM har et høyt dynamisk område. Resultater viser en signifikant reduksjon i dynamisk område når LFM er brukt som spredesekvens. Kompleks Gaussisk støy har stor instantan båndbredde som fører til sterke EK beskyttelses-egenskaper. Det å bruke støy som spredesekvens gir lovende resultater, men i reelle radar- og kommunikasjonsmottakere vil det kreve en høy oppløsning. Fasekodede bølgeformer er bevist effektive for radar, kommunikasjon og EK. De har samme båndbredde som sammenlignbar kompleks Gaussisk støy, men med en konstant amplitude som muliggjør bruken av enklere komponenter.

I tillegg er en multifunksjonell RF system (MRFS) prototype implementert og demonstrert på SDR. Et anti-drone scenario ble valgt for å demonstrere denne prototypen. En bølgeform ble optimalisert for å oppfylle de scenario-definerte kriteriene. Bølgeformen ble implementert basert på simuleringsresultater. Eksperimentelle resultater bekreftet at den fasekodede bølgeformen kunne simultant detektere droner, synkronisere kommunikasjon, og jamme en IEEE 802.11 Wi-Fi link. En 1 W radarimplementasjon var kapabel til å detektere en drone på en avstand av 70 m. På samme tid sendte den modulerte symboler med en bitrate på 1.5 Mbps. 25 MHz instantan båndbredde gav en avstandsoppløsning på 6 m. Bølgeformen var også kapabel til å jamme Wi-Fi linken med et jamme-til-signal forhold på 3 dB. Dette demonstrerer realiseringen av multifunksjon på hyllevare SDR.

Preface

This thesis was written as a conclusion to my 5-year master program at Department of Electronic Systems (IES) at NTNU. The work was carried out during the spring semester of 2017, further developing on the background and simulations performed in the semester project undertaken the fall of 2016. It provides an overview to the vast research topic of multifunctional RF. The topic of multifunction allowed me to delve into the research on both radar, communication, and electronic warfare, while at the same time seeing the bigger picture. The different terminology and primary focus of the research fields is a challenge. The development of software defined systems allows for endless possibilities if the research on the different RF functions are combined. May this thesis be an inspiration for future work, and for the cooperation between research fields.

I would like to express my sincere gratitude to my supervisors at NTNU and FFI. Professor Nils Torbjörn Ekman provided valuable guidance into this research field during the fall semester of 2016, and early 2017. Professor Kimmo Kansanen gave good feedback the last months of this work. I thank Associate Professor UiO and Scientist FFI Jonas Moen for all the support, and for believing multifunctional RF would be an interesting topic. Scientist FFI Thomas Thoresen provided valuable help throughout this work, and I am grateful for all the academic discussions at your office. I must also thank Scientist FFI Jonas Christensen for lending me his radar testbed, and Scientist FFI Dr. Alexander Wold for his brilliant feedback on my writing.

This thesis also concludes 20 years of education. I have learned a lot, and would not have been able to do so without my friends and family. I must thank all my friends for so many wonderful memories these years. My deepest gratitude to my family for all the support. You have provided the best possible foundation for learning and development back home.

Finally, I must especially thank my father Trond Åsheim and grandfather Harald Bjørånesset. The interest in science and engineering came easily with your guidance and knowledge. You are my inspiration and my greatest role models.

Kjeller, July 6, 2017

"Livet er herlig"

Anders B. Åsheim

Acronyms

ACF	auto-correlation function.
ADC	analog-to-digital converter.
AF	ambiguity function.
AMRFC	advanced multifunction RF concept.
AWGN	additive white Gaussian noise.
BER	bit error rate.
BPSK	binary phase shift keying.
CDMA	code division multiple access.
COTS	common-off-the-shelf.
CPI	coherent processing interval.
CW	continuous wave.
DAC	digital-to-analog converter.
DSSS	direct sequence spread spectrum.
EA	electronic attack.
EP	electronic protection.
ES	electronic support.
EW	electronic warfare.
FFI	Norwegian Defence Research Establishment.
FFT	fast Fourier transform.

FOI Swedish Defence Research Agency.

FPGA field programmable gate array.

GPS Global Positioning System.

JSR jammer to signal ratio.

LFM linear frequency modulated.

LPI low probability of intercept.

MF matched filter.

MIMO multiple input multiple output.

ML maximum length.

MRFS multifunctional radio frequency system.

MW multifunctional waveform.

OFDM orthogonal frequency division multiplexing.

PAPR peak-to-average power ratio.

PN pseudo-noise.

PRF pulse repetition frequency.

PRI pulse repetition interval.

PSK phase shift keying.

PSR peak-to-side lobe ratio.

RadCom radar and communication system.

RCS radar cross section.

RF	radio frequency.
RSSI	received signal strength indicator.
SDR	software defined radio.
SNR	signal-to-noise ratio.
SS	spread spectrum.
USRP	Universal Software Radio Peripheral.
WGN	white Gaussian noise.

List of symbols

γ_i = Signal to noise ratio at input
γ_o = Signal to noise ratio at output
λ = Wavelength
δ_R = Sensitivity level
Δf_d = Doppler resolution / Doppler tolerance
Δf_{PD} = Doppler resolution with pulse-Doppler processing
ΔR = Range resolution
σ = Radar cross section
τ_c = Chip duration
ϕ_k = Phase angle
A_e = Antenna effective area
b = Attenuation amplitude
B = Bandwidth
B_{chip} = Chip bandwidth
B_r = Receiver bandwidth
c = Speed of light
C = Channel capacity
d = Degree of polynomial
E_b = Bit energy
E_c = Chip energy
E_s = Symbol energy
E = Pulse energy
f_d = Doppler frequency
f_s = Sampling frequency
F_r = Receiver noise figure
G = Antenna gain
G_t = Transmitter antenna gain
G_r = Receiver Antenna gain
J_0 = Jamming power spectral density
k = Boltzmann's constant
L = Nr of data-symbols
M = Spreading Factor in DSSS
N = Total number of chips in codeword
N_0 = Power spectral density of noise
$n(t)$ = Noise
P_a = Interference power
P_d = Probability of detection
P_e = Probability of error (BER)

P_{fa} = Probability of false alarm
P_N = Noise power
P_t = Transmitter power
P_r = Receiver power
PG_R = Radar processing gain
$r(t_r)$ = Cross correlation
R_b = Bit-rate
R_c = Distance between communication transmitter and receiver
R_{max} = Maximum radar range
R_t = Range to radar target
R_{un} = Unambiguous range
t_d = Time-delay of reflected signal
t_r = Time-variable in correlation receiver
T_0 = Standard noise temperature
T_p = Duration of pulse
T_{int} = Integration time
T_{PRI} = Pulse repetition interval
T_s = Duration of information symbol
v_r = Radial velocity of target
$x_t(t)$ = Transmitted signal
$y_r(t)$ = Received signal

Contents

Chapter 1

Introduction

Network-centric operations require increased sensor capabilities [1]. Compared to traditional warfare scenarios, network-centric operations also requires additional bandwidth. This results in multiple advanced hardware components on the same ship, aircraft or other military platform. Furthermore, electronic warfare (EW) has become an essential tactical feature of current military systems. The ability to hide transmitted signals, detect enemy signals, and react to them is key to survivability [2, 3]. Communication systems demanding higher capacity and bandwidth leads to higher carrier frequency. Some communication systems are close to the frequency spectrum traditionally used by radar applications. As discussed by Erricolo et al. [4], this is a challenge with respect to spectrum sharing. Radar systems are particularly vulnerable to interference. Research into advanced multifunction RF concept (AMRFC) was undertaken in the early 2000's [5, 6] to address some of these challenges. This research identified reduced weight, cost, power consumption, and radar cross section (RCS) as some of the advantages of combining radio frequency (RF) functions into a single device.

In most radar publications *multifunction* is the ability to undertake both search, track, recognition and/or classification of objects. In [7], Skolnik describes multifunctional radar with the use of an active phased array antenna. In Herd et al. [8], these techniques have been applied to civilian air and meteorology services. Current advanced military radar-systems, for example the F-22 fighter radar [9] has similar capability. The antenna of the F-22 incorporates multifunction in the sub-beam approach. In this thesis, the term *multifunction* is described as by Frennberg et al. [10] and Hughes and Choe [5]. They define multifunction as *Radar*, *Communication*, or *EW* as RF functions to be combined in a multifunctional radio frequency system (MRFS).

This thesis presents an analysis of waveform design characteristics for MRFS. The work targets implementation of simultaneous multifunction on low cost and low power common-off-the-shelf (COTS) software defined radios (SDRs). Combining the RF functions communication, radar, and/or EW has the potential to increase spectral efficiency, reduce cost, and reduce the hardware footprint [5].

An MRFS can be implemented according to three distinct design principles (Quan et al. [11]): time-sharing, sub-beams, or signal-sharing. In time-sharing

mode, the system switches between communication, radar and/or EW, while utilizing the same hardware. Time-sharing has the possibility to use an optimized waveform to the currently executing task. It is not however, able to continuously perform radar surveillance at the same time it is performing communication, EW, or other RF functions on the same antenna. Simultaneous operation of different functions requires a sub-beam or signal-sharing system. In Hughes and Choe [5], an MRFS were different functions are distributed as sub-beams on a phased array antenna is presented. The Swedish Defence Research Agency (FOI) methodology report on MRFS (Frennberg et al. [10]) gives an overview of requirements for different MRFS functions. Related research by Tavik et al. [6] and Otten et al. [12], provides comprehensive background on MRFS. Both put emphasis on the use of multifunctional RF-arrays and hardware. Signal-sharing enables concurrent operation of the functions by waveform design. In [13], Levanon investigate the impact waveform design has on radar performance. Levanon reports that waveform design impacts the performance of an MRFS.

Sturm and Wiesbeck [14] takes the signal-sharing approach by focusing on waveform design for a radar and communication system (RadCom). Multifunction research implementing only radar and communication (omitting EW), often denotes the system by the acronym RadCom (or similar). One method to achieve RadCom is to represent different types of radar waveforms as communication symbols. Roberton and Brown [15] implement communication by utilizing the complete sweep of a linear frequency modulated (LFM) radar signal as the communication signal. In [16], Czubiak adjust the pulse repetition frequency (PRF) according to the bit to be transmitted. This technique can be applied to any type of waveform, as the communication receiver only needs to determine what waveform was transmitted. Blunt and Mokole [17] discuss a similar method in detail. However, high bit rates require short waveforms which affects radar performance [14].

Challenges related to waveform design for simultaneous radar and communication function are presented in [14]. The focus is on vehicle to vehicle communication in the 24 GHz band. Sturm and Wiesbeck [14] implement a RadCom system using orthogonal frequency division multiplexing (OFDM). OFDM is widely used in current communication systems [18]. It also has potential as a radar waveform, as reported in [19]. Sit et al. [20] introduce an efficient method of Doppler estimation depending solely the OFDM symbols rather than the whole baseband signal. Other published work [21, 22] exploit OFDM as a solution in bi-static or multiple input multiple output (MIMO) fashion respectively. In Zhao et al. [23], the use of phase coded OFDM signals to achieve RadCom is investigated. Based on the previous research into OFDM in RadCom applications, it appears that OFDM is a promising waveform for MRFS. However, advanced signal processing is required to address the multicarrier structure. Furthermore, OFDM signals are known to have

high peak-to-average power ratio (PAPR) [24]. A high PAPR puts higher demand on power amplifiers to keep them linear. This leads to more expensive implementations. In [25], Thompson and Stralka propose a constant envelope OFDM signal to address the challenge of high PAPR. The proposed solution introduces additional complexity. OFDM is also vulnerable to jamming, as reported in [26]. However, as discussed in [27, 28], the waveform can be optimized to EW environments.

The research by Sturm and Wiesbeck [14] also gives an overview of the spread spectrum single carrier approach as a technique to implement a RadCom system. Spread spectrum communication techniques have traditionally seen more use in high interference environments. Publications [15, 29] present RadCom systems based on the LFM radar waveform. Communication and radar are implemented using dedicated quasi-orthogonal code sequences. In [30, 31], this approach is also discussed, with a more direct spreading of symbols onto the LFM waveform. The fractional Fourier transform based waveform by Gaglione et al. [32, 33] provides both high data rates and good radar performance. However, the RadCom implementation has a high level of complexity.

Spread spectrum communication has properties which are useful to both civilian and military communication. It provides resistance to electromagnetic interference, anti-jamming capabilities, and low probability of intercept (LPI) [34]. It is useful in multiuser mobile communication systems in the form of code division multiple access (CDMA). The technology has been implemented in a wide range of systems [35]. Direct sequence spread spectrum (DSSS) techniques using pseudo-noise (PN) sequences have similarities to the research on noise radar undertaken by Axelsson [36, 37, 38]. The implemented continuous wave (CW) noise radar by Malanowski and Kulpa [39] shows the feasibility of this technique. As discussed by Shaojian et al. [40] and Xu et al. [41], the characteristics of a noise waveform RadCom will have good LPI properties and are resistant to interference and jamming. The DSSS systems demonstrated in [40, 41] are based on CDMA techniques. Different PN sequences for the communication and radar function are used to avoid interference.

In later years, improvements in semiconductor process technology have allowed programmable real-time signal processing algorithms to be implemented digitally. The increased computational power enables digital radar and communication processing to be moved forward in the RF chain. As demonstrated by Gaglione et al. [33], current COTS SDRs have the necessary performance required to implement MRFS functionality.

The concept analyzed in this thesis is what degrees of freedom are available when implementing multifunctional waveforms (MWs) for an MRFS. Simulations of different design techniques are presented, as well as a demonstration of an MRFS. Before designing an MW, performance criteria needs to be identified. An under-

standing of how design decisions affect them are also required. This thesis expands on previous research in this area. At the same time, the EW aspect is also considered, emphasizing the use of single carrier broadband waveforms.

The properties of DSSS sequences and noise-like waveforms are investigated in detail in this thesis. Taking the signal-sharing approach [11], a waveform based on DSSS directly as communication and radar is further analyzed. The waveform design is based on the work on spread spectrum RadCom by Sturm and Wiesbeck [14]. However, in this thesis the EW aspect is also considered, as well as inclusion of long-coding technique for spread spectrum. The waveforms can be digitally generated, and processed on an SDR. Spreading by LFM sequences, PN phase codes and white Gaussian noise (WGN) are analyzed further. Binary phase shift keying (BPSK) is the modulation technique used in this thesis. The basis of the discussion based on binary phase sequences provides an introduction and explanation on MW design. Polyphase codes discussed by Pace [3] has radar-processing advantages compared to binary phase codes. The waveforms are evaluated for communication, radar and EW performance in a MATLAB analysis and simulation tool implemented for this purpose. Some of the waveforms are used in experiments on a B210 SDR from Ettus Research [42] and the radar testbed by Christiansen et al. [43]. This is to demonstrate the multifunctional capability of simultaneous radar, communication, and EW implemented on a COTS SDR.

1.1 Structure of this Thesis

The remainder of the thesis is organized as follows: Radar, communication, and EW theory are presented in chapter 2. This form a basis for performance, and defines the degrees of freedom available when implementing an MRFS. In chapter 3, design considerations are discussed and simulated to quantify effects of design decisions. Performance parameters are tied to waveform design variables using the theory from chapter 2. Furthermore, MATLAB simulations show some of the differences between different MW's. Scenarios where the use of an MRFS has potential are presented in chapter 4. This gives further motivation to this research area. In chapter 5, a prototype system and waveform design based on one of the scenarios is presented. In addition, the chapter present experiments that demonstrate the capabilities of the implementation. Finally, in chapter 6, the conclusion and future work is presented.

Chapter 2

Theory and Background

2.1 Radar

A radar is a system that emits electromagnetic waves to detect and localize objects. Figure 2.1 shows the principle of a basic radar system with separate transmit and receive antennas. As the transmitted signal propagates through the air it will be attenuated. If the target or radar are moving relative to each other, a Doppler-shift is induced. When the reflected signal returns to the receiver a detection is made. Range to the target is computed based on the time used.

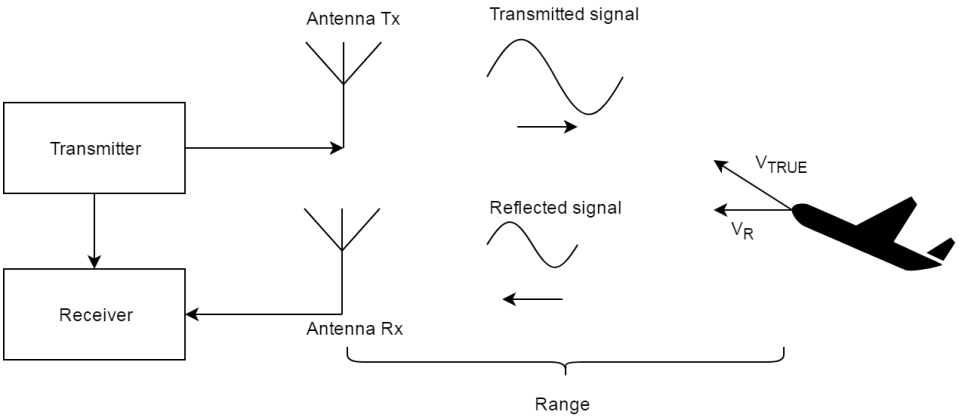

Figure 2.1: Basic radar transmitting an electromagnetic waveform from a transmitter, and receiving the reflected echo from a target on a receiver

2.1.1 Range and the Radar Equation

If the transmitted signal is a pulse, or rather a train of pulses, it represents a traditional pulsed radar with a given pulse repetition interval (PRI). The radar PRI must be sufficiently long for the pulse to return before a new pulse is transmitted to avoid unambiguous detections. If a reflection from a target at long range returns after a new pulse is transmitted, it will appear as much closer than it is. The

maximum unambiguous range is given by [7]:

$$R_{un} = \frac{cT_{PRI}}{2} \tag{2.1}$$

where $c \approx 3 \times 10^8$ is the speed of light. The maximum unambiguous range gives the interval T_{PRI} between pulses, it does not give the upper limit to how far away a radar can detect objects. A signal or pulse with peak power P_t is transmitted from an antenna with gain G_t and propagates through the air towards a target with radar cross section σ and distance R_t. The reflected pulse will return to the receiver antenna with power of:

$$P_r = \frac{P_t G_t A_e \sigma}{(4\pi)^2 R_t^4} \tag{2.2}$$

Where A_e is the effective area of the antenna. It depends on the wavelength λ of the transmitted pulse. By substituting the antenna area with the receiver antenna gain $G_r = 4\pi A_e/\lambda^2$ we obtain the classical *Radar Equation* derived in Skolnik [7]:

$$P_r = \frac{P_t G_t G_r \lambda^2 \sigma}{(4\pi)^3 R_t^4} \tag{2.3}$$

The received power needs to be amplified by the receiver. This introduces noise into the system. The receiver requires a certain minimum input signal power to detect a target. The sensitivity level δ_R substitutes the input power P_r in Equation 2.3 and represents the minimum signal-to-noise ratio (SNR) required at the input γ_i, multiplied with the input noise power at the receiver.

$$\delta_R = kT_0 B_r F_r \gamma_1 \tag{2.4}$$

where k is Boltzmann's constant, $T_0 = 290$ K the standard noise temperature, B_r the receiver's input bandwidth, and finally F_r the receiver noise figure. Rearranging Equation 2.3, the maximum detection range for the radar becomes:

$$R_{max}^4 = \frac{P_t G_t G_r \lambda^2 \sigma}{(4\pi)^3 k T_0 B_r F_r \gamma_i} \tag{2.5}$$

It is common in radar processing to use integration or other pulse compression techniques to improve detection capabilities. Signal processing of the radar waveform relates the input SNR γ_i and the output SNR γ_o by the *processing gain*:

$$PG_R = \frac{\gamma_o}{\gamma_i} \tag{2.6}$$

The processing gain depends on the integration of pulses and the time-bandwidth properties of the waveform. The output SNR can be related to design specific parameters such as Probability of False Alarm P_{fa} and Probability of Detection P_d with Albersheim's empirical formula [44]:

$$\gamma_o = A + 0.12AB + 1.7B \tag{2.7}$$

where

$$\begin{aligned} A &= ln[0.62/P_{fa}] \\ B &= ln[P_d/(1-P_d)] \end{aligned}$$

The minimum range depends on the radar system setup. If the two antennas shown in Figure 2.1 do not have sufficient isolation there will be interference. A traditional method to address this problem is to turn off the receiver when transmitting. This is also the case in a radar system using only one antenna for transmit and receive [7]. Target returns from the time the receiver is turned off is ignored, and the radar is *eclipsed*. In a CW radar system interference is reduced by isolating the antennas properly, using directive antennas and reducing the transmit power.

Other interfering signals can come from unwanted target returns called *clutter* [7, 45]. These are often large reflections can mask the targets the radar is looking for, although in a different way than random noise. A method of addressing clutter (and other radar interference) is using a constant false alarm rate detector as described in Richards et al. [45, Chapter 16].

The received signal $y_r(t)$ reflected off a point target is a delayed and attenuated version of the transmitted signal $x_t(t)$:

$$y_r(t) = bx_t(t - t_d) + n(t) \tag{2.8}$$

where b is a constant attenuation amplitude, and $n(t)$ is noise. The radar range R_t to an object is calculated from the time t_d it takes the transmitted signal to travel to, and be reflected off the target:

$$R_t = \frac{ct_d}{2} \tag{2.9}$$

where c is the speed of light. In other words, range is estimated by measuring the time delay t_d.

2.1.2 Matched Filter and Range Resolution

In many radars range is estimated by finding the lag of the maximum value in the cross-correlation between the transmitted signal $x_t(t)$ and the received signal $y_r(t)$:

$$r(t_r) = b \int x_t(t - t_d) x_t^*(t - t_r) dt + \int n(t) x_t^*(t - t_r) \tag{2.10}$$

where $(^*)$ is the complex conjugation. When $t_r = t_d$ a peak will occur, and the range R_t can be calculated. In a digital system t_r is a discrete value. The transmitted signal will also be a discrete sequence of samples. The synchronization of received samples, and reference samples will enhance the detection capability.

Cross-correlation, or auto-correlation function (ACF), introduces sidelobes. The peak-to-side lobe ratio (PSR) in range is an important parameter when analyzing waveform capabilities. PSR represents the magnitude from the peak $r(0)$ down to the highest of the sidelobes max $r(t_r)$ in Equation 2.10 and is defined as [45]:

$$\text{PSR} = 10 \log \left[\frac{\max\, r^2(t_r)}{r^2(0)} \right] \tag{2.11}$$

Waveforms with low PSR may mask smaller target returns in range cells corresponding to the sidelobes. Reducing these sidelobes, with weighting functions or filters are discussed in detail in Richards et al. [45].

Another challenge with range estimation is the ability to distinguish two separate targets, or in other words the range resolution. The transmitted signal x_t used in the cross-correlation represents a matched filter (MF).

Instead of sending short high-power pulses, performance can be improved by shaping the radar waveform. As presented in Gini et al. [46], the transmitted waveform is used in the correlation receiver, so the sidelobes of the correlation and range resolution is highly dependent on the design of the radar waveform (or the MF of that waveform). Using a MF is known as pulse compression and is achieved by modulating the waveform. The bandwidth of the pulse increases, and it behaves like a short pulse at the output of the MF. The gain achieved by pulse compression is defined by the Time-Bandwidth product (T_pB) of the waveform. It relates to the processing gain in Equation 2.6. Figure 2.2 shows the output of a MF response of an LFM waveform. This is the same as the ACF when $t_d = 0$ in Equation 2.10. The peak of the MF response represents the point when $t_r = t_d$ in Equation 2.10.

It is proportional to the energy E in the transmitted waveform of duration T_p:

$$E = \int_0^{T_p} |x_t(t)|^2 dt = P_t T_p \tag{2.12}$$

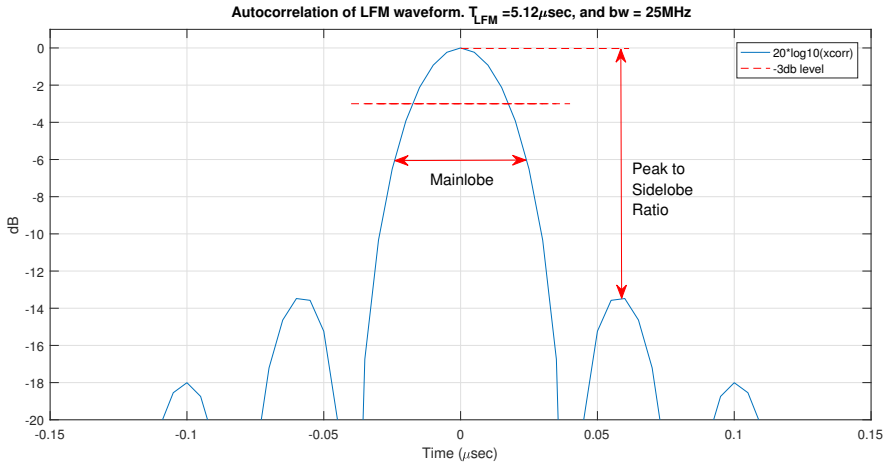

Figure 2.2: Autocorrelation of a LFM waveform with a Time-Bandwidth product of 128

For pulse compression waveforms with a MF at the receiver, the receiver bandwidth equals the bandwidth of the transmitted waveform ($B_r = B$). The correlation time of the MF $T_{int} = T_p$ the pulse length. The Radar Equation 2.5 is reduced to [45]:

$$R_{max}^4 = \frac{P_t G_t G_r \lambda^2 \sigma}{(4\pi)^3 k T_0 B_r F_r \gamma_o} T_p B = \frac{E G_t G_r \lambda^2 \sigma}{(4\pi)^3 k T_0 F_r \gamma_o} \tag{2.13}$$

In Richards et al. [45, chapter 20], range resolution is defined in multiple ways, including the -3 dB main lobe width depicted in Figure 2.2. For pulse compression waveforms, a good range resolution approximation with respect to the bandwidth is:

$$\Delta R = \frac{c}{2B} \tag{2.14}$$

2.1.3 Doppler and Ambiguity Function

In Figure 2.1, a radial velocity v_r of the target introduces a Doppler shift f_d to the reflected waveform:

$$f_d = \frac{2v_r}{\lambda} \tag{2.15}$$

The received waveform from Equation 2.8 will now be on the form:

$$y_r(t) = bx_t(t - t_d)\exp(j2\pi f_d t) \tag{2.16}$$

This results in a mismatch between the reflected waveform and the MF. The characteristics of this mismatch, and the MF's response to Doppler is defined by its ambiguity function (AF) [47]:

$$\chi(t_d, f_d) = \left| \int x_t(t)x_t^*(t - t_d)\exp(j2\pi f_d t)dt \right| \tag{2.17}$$

The AF has many defining properties for the waveform. It is a tool to evaluate and compare different waveforms. The AF of an LFM waveform is shown in Figure 2.3. The surface plot of the 2D AF is a visual representation of the MF response. The zero-Doppler cut ($f_d = 0$) represents autocorrelation in Figure 2.2. The AF shows degradation of the response for a Doppler-shifted reflection. As presented by Richards et al. [45], both the peak amplitude, main lobe width and PSR are affected. The LFM waveform is *Doppler tolerant* due to its diagonal ridge in the AF. A high uncompensated Doppler shift is still passed through the MF, making detection possible, although degraded.

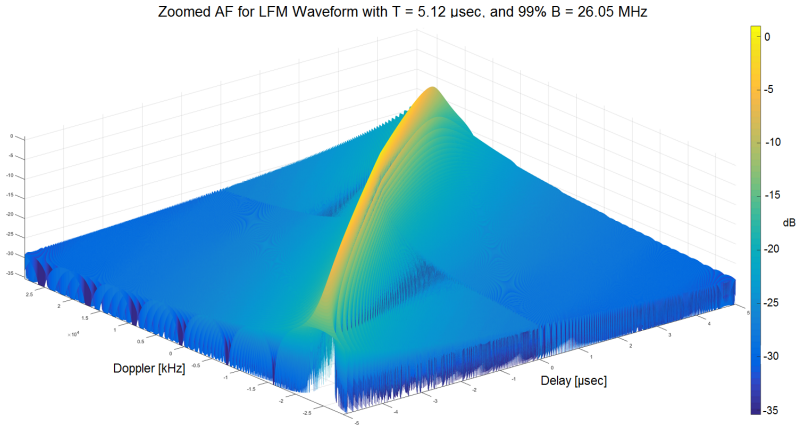

Figure 2.3: The AF of a LFM waveform.

Doppler processing enables the radar to detect moving targets in a dense clutter environment. The Doppler shift can also be used to compute the radial velocity of the target. *Pulse-Doppler processing* is a method that, based on multiple returned reflections, computes the Doppler of targets using the fast Fourier transform (FFT). This is depicted in Figure 2.5 over a coherent processing interval (CPI). A total of M_p returned pulses with a PRI of T_{PRI} are stacked in slow-time as shown in Figure 2.4 resulting in a Doppler resolution of:

$$\Delta f_{PD} = 1/M_p T_{PRI} \tag{2.18}$$

Each fast-time bin represents one range cell, and FFT can be performed to process out Doppler. This is usually much fine-grained than the theoretical Doppler resolution $1/T_p$ of one pulse [45]. Combining Equation 2.18 and Equation 2.15 results in a radar velocity resolution of:

$$\Delta v_r = \frac{\lambda}{2M_p T_{PRI}} \tag{2.19}$$

The sampling rate in Slow-Time is the inverse of the PRI called PRF. The Nyquist sampling theorem states a maximum unambiguous Doppler shift will be $\pm PRF/2$, or the maximum unambiguous velocity v_{un} given by:

$$v_{un} = \frac{\lambda}{2T_{PRI}} \tag{2.20}$$

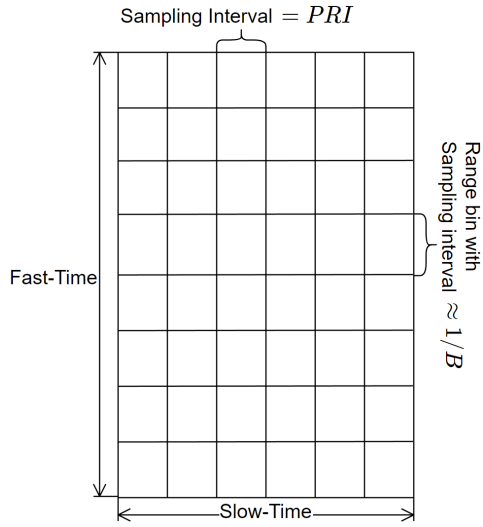

Figure 2.4: Fast-time and slow-time stacking of received radar pulses.

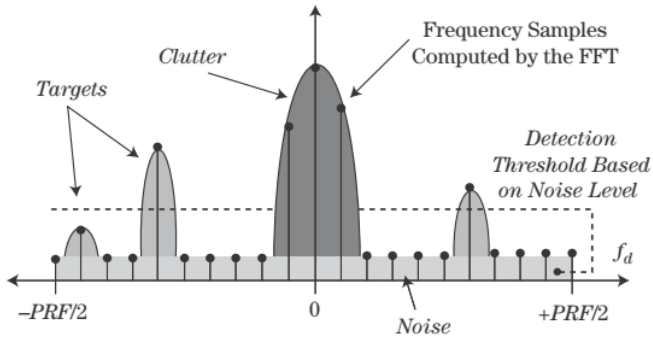

Figure 2.5: The concept of pulse-Doppler processing. Figure from [45]

With knowledge of the expected target velocity, the waveform can be designed to be Doppler tolerant within the expected Doppler shifts. With high velocity targets, or increased range resolution one may experience *range walk*. A method to remove Doppler and address range walk is to use a filter bank of mismatched receivers. The mismatched filters are configured as Doppler shifted MFs according to the Doppler tolerance of the waveform. Different implementations of this concept are reviewed in Xu et al. [48].

2.1.4 Radar Waveforms

Radar waveforms can be generated and modulated in numerous ways. This is presented in Blunt and Mokole [17]. It is classified into the four categories: frequency modulated, phase coded, frequency coded and random noise. In addition, the waveforms can either be pulsed or CW. A CW operated radar can be considered pulsed radar with duty cycle of 100 % or $T_{PRI} = T_p$ [17].

LFM

The LFM waveform, commonly called *chirp*, is one of the most used waveforms in radar today [49]. This is due to exhibiting high Doppler tolerance and linear relationship between time and Doppler frequency as depicted in Figure 2.3. An example LFM waveform is shown in Figure 2.6. The time plot shows the linearly increasing frequency of the sine. The frequency can be increased up, down or as a triangle. The LFM waveform can cover a large bandwidth increasing the range resolution. It has a limited instantaneous bandwidth due to its linear nature as shown in the spectrogram.

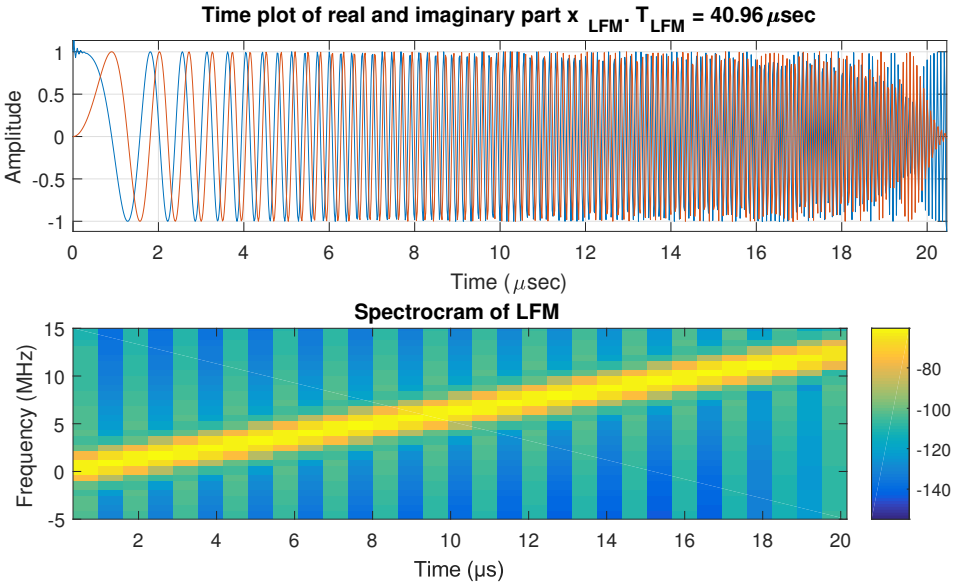

Figure 2.6: The characteristics of an LFM waveform. Time plot and spectrogram.

Phase-Coded Waveforms

Another well-known pulse compression technique is phase shift keying (PSK) [3]. Phase coded waveforms consist of elements called *chips* of duration τ_c. Several chips are put together to form a codeword of length N. An example of a binary phase-coded waveform is the Barker 13 in Figure 2.7. The allowed states for ϕ_k is 0 or 180 degrees, with amplitudes given by $\exp(j\phi_k) = \pm 1$. The range resolution of an appropriately chosen phase code is given by the chip duration, as the -4 dB bandwidth $B_{chip} = 1/\tau_c$ for rectangular chips [45]. The coding sequence greatly affects performance. The PSR is given by the choice of codeword. The best performing PSR with a defined code length is the Barker 13 with a PSR of $1/N$ or -22.3 dB [50]. This PSR is depicted on the bottom of Figure 2.7. The total duration of the PSK waveform is $T_p = N\tau_c$, thus the time-bandwidth product is directly related to the codeword length as:

$$T_p B = N\tau_c B_{chip} = N \tag{2.21}$$

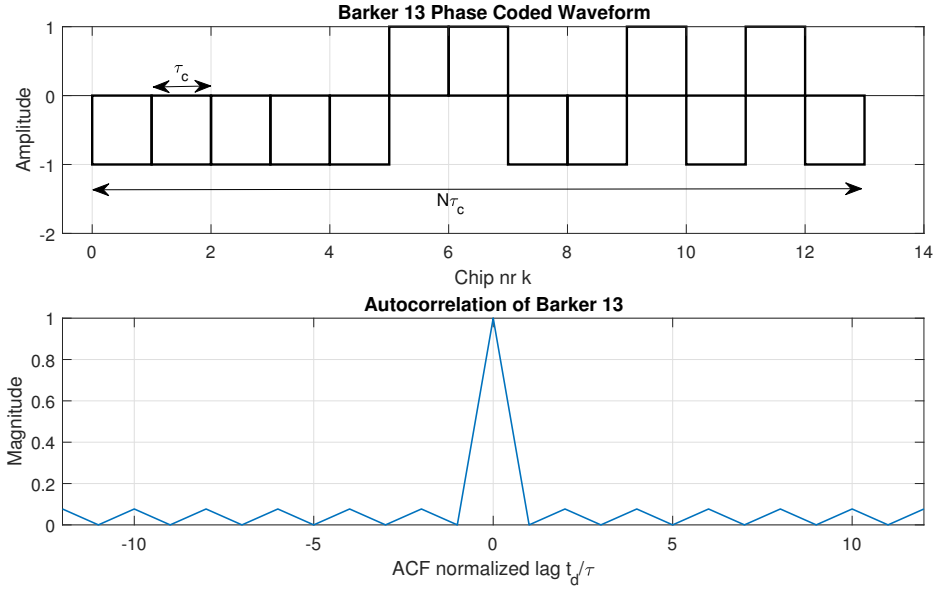

Figure 2.7: Barker 13 waveform on top. The amplitude represents a phase shift as $A = \exp(j\phi_k)$. On bottom, the autocorrelation of Barker 13.

The MF response of phase coded waveforms degrade quickly in the presence of Doppler. In the zero-time cut of the AF ($\chi(0, f_d)$), the phase coded waveforms have the shape of a sinc, with the first null at $f_d = 1/N\tau_c$ [45]. A good approximation for the Doppler resolution of a radar waveform is the inverse of the pulse duration:

$$\Delta f_d = \frac{1}{T_p} = \frac{1}{N\tau_c} \tag{2.22}$$

Longer codes will therefore resemble a thumb tack shape, as the sinc main lobe is narrower with increasing code length as seen in Figure 2.8. Binary phase codes are Doppler intolerant due to this property. Waveforms with a thumb tack shaped AF can detect target range and Doppler simultaneously, using a bank of mismatched filters. Each of the mismatched filters are Doppler shifted. The filter with the highest response is associated with the target Doppler.

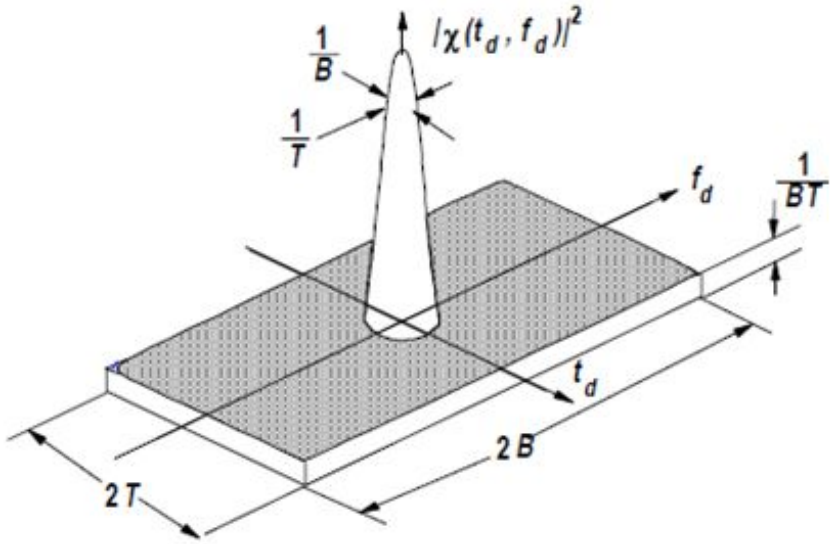

Figure 2.8: The theoretical AF of a noise-like waveform from [51]. B is the bandwidth, and T the pulse duration and gives the range resolution and Doppler resolution respectively.

Maximum Length Bi-phase Waveforms

Although Barker codes has the lowest PSR for a certain length, there are no Barker codes longer than $N = 13$ [45]. Maximum length (ML) sequences are codewords that exhibit good PSR approaching $10\log_{10}(1/N)$. The binary sequences are of length $N = 2^d - 1$, where d is an integer and the degree of the ML sequence. Figure 2.9 shows the zero cut of the AF for a ML sequence of length $N = 1023$. The sidelobes are lower close to the main lobe and increases towards -30 dB. In Doppler, the first null appears at $f_d \approx 48kHz$ in accordance with $\Delta f_d = 1/N\tau_c$. The ML sequences are efficiently implemented using shift registers, and a corresponding *primitive polynomial*. In [52], Dinian et al. describes generation and theory of ML sequences.

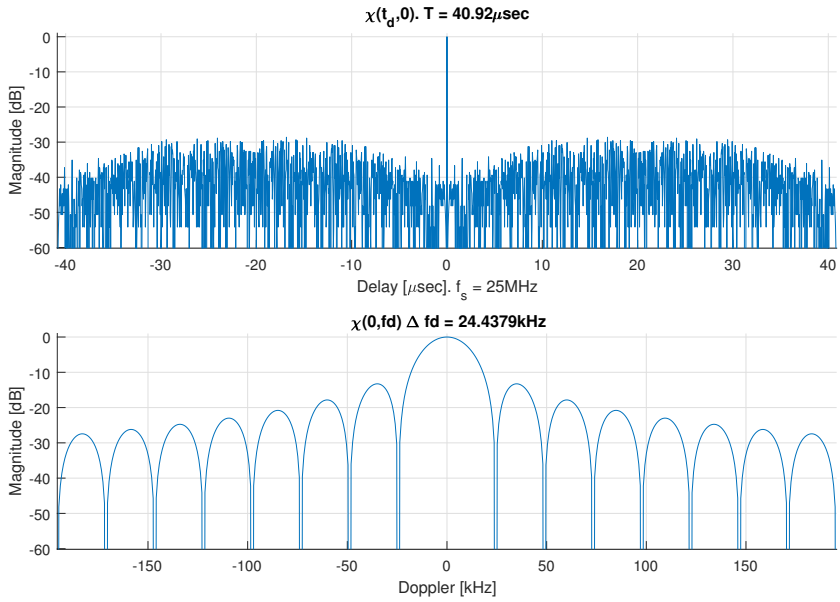

Figure 2.9: Zero cut in Doppler $f_d = 0$ (at the top) and time $t_d = 0$ (bottom) for a ML sequence of length $N = 1024$ with a sample rate of $f_s = 50$ MHz

2.1.5 Noise Radar

The concept of noise radar was introduced late in the 1950's by Horton [53]. Implementation of noise radars were challenging due to its wideband waveform requires and correlation circuits. Modern digital signal processing and digital-to-analog converter (DAC) circuits make it possible to implement most of the processing digitally. Noise radar can detect range and Doppler. In addition, it is resistant to interference and jamming [38]. The drawback with noise radar however, is the reduced dynamic range. This is because the MF generates a noise floor below the peak response as shown in Figure 2.8. Usually noise radar is implemented as a form of non-repeating CW radar as presented by Malanowski and Kulpa [39]. The AF of a noise radar waveform reassembles a "perfect" thumb tack. The research by Axelsson [36, 37, 38] provides an in-depth study of these waveforms and their characteristics.

In a military scenario "To see and not be seen" is a significant advantage in an operative radar system. LPI characteristics of radar are a major research topic. Many aspects of both LPI radar and noise radar are covered in Pace [3]. Pace gives the following definition of LPI:

> A LPI radar is defined as a radar that uses a special emitted waveform intended to prevent a non-cooperative intercept receiver from intercepting and detecting its emission.

Noise radar uses noise as a special emitted waveform and can lower its transmit power, increase bandwidth, or vary frequency to further emphasize the LPI characteristics.

2.2 Wireless Communication

Wireless communication systems have three figures of merit: *Coverage, capacity*, and *quality* [54]. The properties of the wireless channel will determine all the possibilities and limitations of these three goals. Channel fading effects like path loss and shadowing affects the coverage and capacity, while fast-fading mostly affects the quality. A communication receiver must first achieve synchronization before it can perform any kind of processing on the received sequence. Synchronization is performed by transmitting a known *preamble*, a sequence the communication receiver constantly correlates on. Choosing a preamble with high PSR gives a higher peak for synchronization circuits to detect. The preamble can also be used to perform channel estimation to overcome fading effects. This thesis assumes no other fading effects than free space path loss.

Coverage is the ability to cover an area with enough signal power to receive data. In a free space point-to-point communication channel, the average signal power $\bar{P}_r$ at the receiver with a distance R_c from the transmitter is given by [55]:

$$\bar{P}_r = \frac{P_t G_t G_r \lambda^2}{(4\pi)^2 R_c^2} \tag{2.23}$$

where

P_t = Total transmitted power
G_t = Transmitter Antenna gain
G_r = Receiver Antenna gain
λ = Carrier frequency wavelength
R_c = Distance between transmitter and receiver

When the receiver then amplifies the received signal, noise is introduced to the system. This affects both the capacity and the quality of the system. Capacity is the ability to transmit data through the communication channel, possibly to multiple users. In a single user scenario, it will be the maximum bit rate the system is able to transmit to that user error free. The *theoretical* upper limit to the amount of data to be transmitted through a noisy channel is the Shannon Channel capacity [56]:

$$C = B \log_2 \left(1 + \frac{\bar{P}_r}{P_N}\right) \tag{2.24}$$

B being the channel bandwidth which is the receiver bandwidth, B_r. $\bar{P}_r$ is the average received signal power. P_N is the noise power. The total noise power depends on the receiver bandwidth, as with the radar receiver. As reported in Poisel [2, Chapter 2], at carrier frequencies above 1 GHz, the total noise power is given by:

$$P_N = N_0 B_r + P_a \tag{2.25}$$

where P_a is external noise or interference in the same frequency band as the receiver.

The bandwidth affects the available bit rate, modulation and error correction/detection schemes employed (coding). The BPSK modulation scheme has a maximal spectral efficiency of 1 bit per second per Hertz (bps/Hz) for high SNR. This is also the theoretical upper limit and requires further coding and power allocation in a real-world system. Constellation constrained capacity gives a more defined channel model, reviewed in [57], but this extends beyond the scope of this thesis. Increasing the modulation will increase the spectral efficiency, but it will also increase the sensitivity to noise and interference. The result is a reduction in the quality of the transmission.

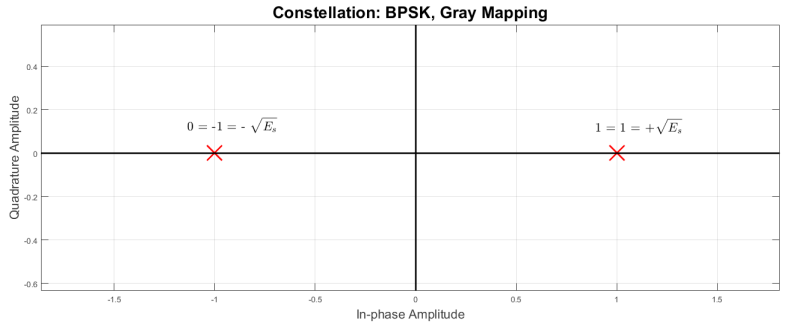

Figure 2.10: Constellation of BPSK.

BPSK maps data bits to symbols according to the constellation diagram in Figure 2.10. Each symbol of duration T_s has the symbol energy $\sqrt{E_s}$, which for BPSK is equal the energy per bit $E_s = E_b$. Transmitting uncoded BPSK symbols in an additive white Gaussian noise (AWGN) channel results in a bit error rate (BER) of [2]:

$$P_e = Q\left(\sqrt{\frac{2E_s}{N_0}}\right) \tag{2.26}$$

where $Q(.)$ is the Q-function for tail probability of standard probability distribution (see Poisel [2, Appendix A]), E_s the *symbol*-energy and $N_0 = kT_0$ the power spectral density of the noise. The theoretical BER for BPSK with the available SNR (Signal-to-Noise Ratio) can be seen in Figure 2.11

2.2.1 Direct Sequence Spread Spectrum

The principle of DSSS is presented in Rappaport [18, chapter 6] or in Pickholtz et al. [35]. The information symbols are spread over a wide bandwidth, usually with a binary PN code. One data-symbol of duration T_s in a sequence $m[l]$ of length L forms symbols to be spread by a spreading sequence $pn(n)$ of length M. The spreading sequence contain M *chips* each of duration τ_c where $\tau_c = T_s/M$. M is referred to as the *spreading factor*. Spreading with binary PN can be done with an exclusive OR operation and generates a spread sequence $x[n]$ of total length $N = M \times L$. Figure 2.12 shows 4 data symbols being spread by a PN-sequence (in this case a ML code) of length $M = 16$ to generate a spread sequence $x[n]$ of length $N = 16 * 4 = 64$.

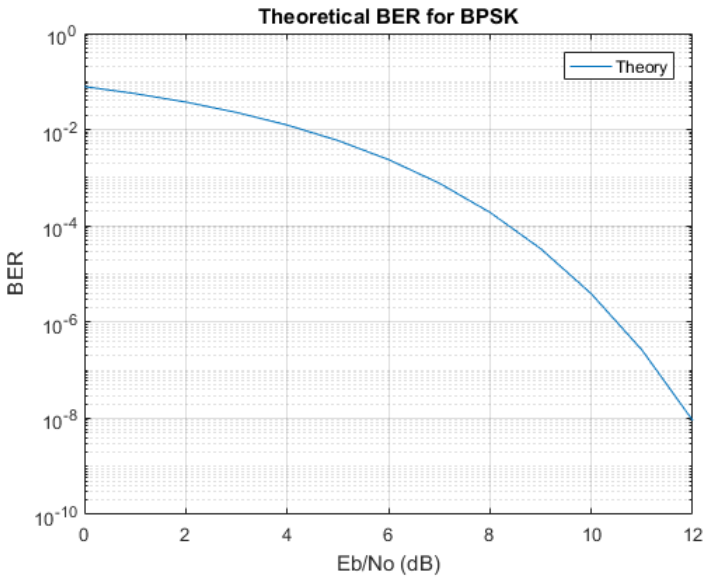

Figure 2.11: Theoretical BER for BPSK

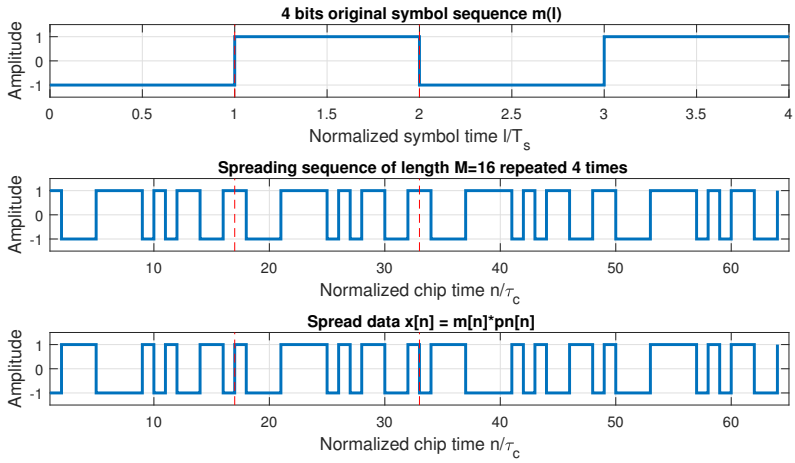

Figure 2.12: Direct Sequence spreading of data symbols

At the receiver, the sequence is de-spread using the same code as used by the transmitter. Assuming perfect synchronization each received symbol is integrated over the symbol time $T_s = M\tau_c$ and a decision can be made on what symbol was transmitted. For a given transmit power P_t the energy in one chip will be $E_c = P_t\tau_c$. M chips represent each symbol, so the processing gain for DSSS systems is given by the spreading factor M. The resulting symbol energy will be given by:

$$E_s = ME_c = MP_t\tau_c \tag{2.27}$$

and the symbol SNR will be given by:

$$\frac{E_s}{N_0} = \frac{E_c}{N_0} + 10\log(M) \tag{2.28}$$

The duration T_p of the sequence $x[n]$ of total length $N = LM$ will be given by:

$$T_p = LM\tau_c = N\tau_c \tag{2.29}$$

Normally M is chosen large so $\tau_c \ll T_s$ [34]. Pickholtz et al. [35] discusses spreading factors in the order of 10-30 dB, meaning the power of the original data-symbols will be spread out to a bandwidth 10-1000 times larger. The spreading factor will make the symbol duration longer, giving a higher symbol energy $E_s = \bar{P}_r M\tau_c$ at the receiver. Altering Equation 2.23 gives an equation for free space loss communication range with spread spectrum:

$$R_c^2 = \frac{P_t\tau_c G_t G_r \lambda^2 M}{(4\pi)^2 k_B T_0 \gamma_r} \tag{2.30}$$

where $\gamma_r = E_S/N_0$ is the SNR required for a certain BER at the receiver.

If $x[n]$ is BPSK modulated and transmitted as a pulse with a PRI of T_{PRI} the output bit rate R_b of the transmission will be:

$$R_b = L/T_{PRI} = \frac{T_p}{M\tau_c T_{PRI}} \tag{2.31}$$

and choosing the correct balance between spreading, PRI, and pulse-duration will give the required the bit rate. Another method to do spreading is to generate a Long-code of length N and chopping that up in L pieces of length M, where $ML = N$. This will improve the sequence $x[n]$'s MF properties as it is not periodic within itself [58].

2.2.2 Pseudo-Noise Codewords

Pure random bit-streams or "codewords" is not deterministic and will not be optimal for a communication system. The concept of pseudo-noise can be reviewed in [18], and is essentially a sequence generated deterministically, but with some statistical properties of randomness. In Dinan and Jabbari [52] different spreading codes for DSSS are reviewed. ML sequences have good auto-correlation properties like narrow peak and good PSR, important attributes to recognize a single coded pulse in noise. Gold (or Kasami) sequences will have better cross-correlation properties, and Walsh-codes have perfect orthogonality, both important features in a multiple access system.

2.3 Electronic Warfare

The concept of EW spans a wide field of study including electronic attack (EA), electronic support (ES) and electronic protection (EP). EA is the use of signals to actively suppress or deny enemy communication, radar, or other form of electromagnetic aggression. ES is the detection, collection, and classification of enemy signals to support EA or use it as intelligence. Everything that prevents an adversary to use EA or ES against you is EP. A non-cooperative receiver trying to detect transmissions (enemy ES) may use different strategies to process out the transmitted waveforms to perform detection and classification. A technique of countering that will be to transmit waveforms that looks like noise, as they will be more difficult to distinguish from the real noise of the non-cooperative receiver. Other examples of EP can be to widen the bandwidth and reducing transmitted power to hide radar/communication waveforms, or using long codewords to encrypt and mask communication (and vice versa). Note that EP and LPI are acronyms that *in this thesis* describe somewhat the same features and characteristics. For more on terms, features and theory of EW see Poisel [2].

Jamming is an EA technique of placing signal power in the same frequency range as the target communication system operates in. The jammer carrier signal is modulated around the target carrier signal, to increase the interference, reduce capacity and force error. Wideband noise jamming is a method of adding broadband noise within the same frequency spectrum the target system. Often called *barrage jamming*, this technique is effective when there is no knowledge of the target system [2]. With prior knowledge of target receivers, other techniques analyzed in [2] are more effective. Barrage jamming essentially increases the noise level at the target receiver. The maximum channel capacity from Equation 2.24 of the transmission is reduced. The additional noise power P_a in Equation 2.25 can now

be represented by the level of jamming power at the target receiver, referred to as J_0 and measured in watts/hertz. The parameter often associated with jammer performance is jammer to signal ratio (JSR), the power relation between the jammer signal and the communication signal at the target receiver. Assuming the noise power covers the entire bandwidth of the receiver, Equation 2.25 is rewritten to:

$$P_N = B_r(N_0 + J_0) \tag{2.32}$$

The added jammer power also affects the BER of the transmission, and Equation 2.26 is adjusted accordingly:

$$P_e = Q\left(\sqrt{\frac{2E_s}{N_0 + J_0}}\right) = Q\left(\sqrt{\frac{2E_s}{N_T}}\right) \tag{2.33}$$

where $N_T = N_0 + J_0$ the total noise power spectral density at the target receiver. It must be noted that Equation 2.33 holds for simple symbol transmission. For communication systems, there often exist a processing gain as discussed in section 2.2. For a broadband jammer, this means the jamming power must overcome the processing gain before the BER on the receiver really starts to increase [2, chapter 10]. Jamming of OFDM communications are discussed in [59]. Shahriar presents a baseline BER of 0.1-0.4 to break down a OFDM link.

In a pulsed system, the jammer performance will naturally be limited by the time the transmission is off. The jamming pulse duration T_p must be at least one bit time for the receiver system to experience significant BER. Compared to a non-pulsed jammer, the peak power must also increase to have the same average power. Pulsed jamming techniques of DSSS systems has an advantage when the E_s/N_T is above a certain threshold [2]. However, with same *average* power and bandwidth as the non-pulsed jammer.

2.4 Multifunction on Software Defined Radios

One of the core concepts of most of the MRFS are that the waveforms are implemented digitally and on an SDR. In an SDR the transmitted signals are formed in software. The received signals are sampled at an early stage in the receiver chain, often after a suitable band selection filter [60]. Most SDR's today can perform coherent detection [61], a property important for many of the assumptions done in this thesis. An example block diagram of the Ettus Research Universal Software Radio Peripheral (USRP) B210 are depicted in Figure 2.13. A computer can be connected to program and transfer data to and from the SDR. The digital signal

processing units are implemented on a field programmable gate array (FPGA). The integrated RF-integrated circuit are where the DAC and analog-to-digital converter (ADC) are, sampling data at a rate up to 56 MHz and 12-bit resolution.

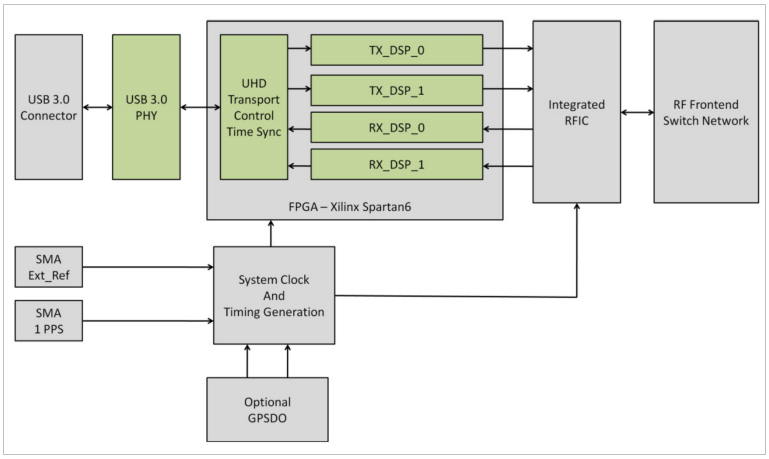

Figure 2.13: The block diagram of the Ettus Research B210 SDR from [42].

Most SDRs are dependent on a power amplifier in the transmit chain. Presented by Tsouri and Wulich [62], if the waveform has a high PAPR it will require a linear power amplifier with large dynamic range. The power amplifier will be less power efficient when the dynamic range requirement increases. In the case of non-linearity, the waveform will be distorted and spread in frequency.

A great advantage with software defined systems is the ability to change parameters continuously. Cognitive radio (or radar) discussed in [43, 63, 64] is a new interesting field of study. With knowledge about the environment the cognitive system can adjust the parameters of the waveform. This will enable the waveform to best suit the wanted performance or objective.

Chapter 3

Waveform Design

This chapter first presents the figures of merit for communication-, radar-, and EW-functions. Then the general waveform design variables and how these affects performance in an MRFS are analyzed. Furthermore, the MATLAB tools created are presented before the conceptual spread spectrum MWs are analyzed and simulated.

3.1 Figures of Merit

3.1.1 Radar Performance

Radar system performance can be characterized by the following [10]:

- Range and Doppler detection
- Total range (from the Radar Equation 2.5)
- Range resolution
- Doppler tolerance/resolution
- Unambiguous range
- LPI

The maximum range R_{max} of a radar system will be limited by the radar Equation 2.5, but also the unambiguous range R_{un} from Equation 2.1. The two equations links together hardware specific constraints with design choices. Antenna gain G and receiver noise figure F_r are hardware specific parameters. Probability of detection P_d and false alarm P_{fa} are requirements which by Equation 2.7 give the required SNR.

Doppler tolerance or resolution depends on the type of Doppler processing performed by the MRFS. The two methods are depicted in Figure 3.1. Traditional pulse-Doppler processing from Equation 2.19 will depend on the CPI used. The waveform must also be sufficiently Doppler tolerant, as target returns with a Doppler shift above $max\Delta f_{PD}$ will be heavily attenuated. For single-pulse Doppler

processing performed by having a bank of mismatched filters, the inverse is the case. Creating a waveform with low Doppler tolerance makes the resolution Δf_d finer, as the filters can be created with smaller gaps.

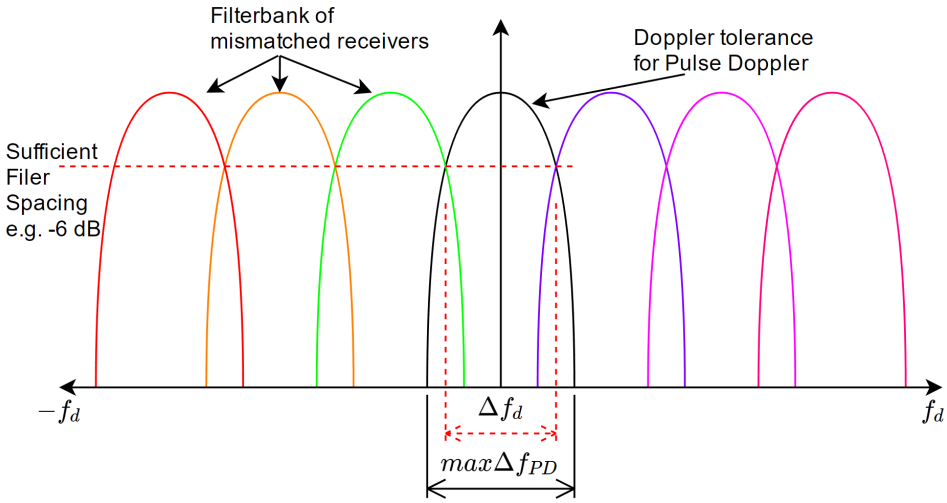

Figure 3.1: Filter bank of mismatched filters with spacing according to the Doppler tolerance of the transmitted waveform. Traditional pulse-Doppler processing will be limited by the Doppler tolerance of a single matched filter in the center.

3.1.2 Communication Performance

For a communication system performance is described by the following [10]:

- Capacity/bit rate
- Coverage and range
- Quality (BER)
- Power consumption

In addition, there are military criteria linked to:

- Stealth performance (LPI)
- Resistance to interference and jamming

Shannon's channel capacity Equation 2.24 will give the maximum error free capacity, and the output rate R_b should be limited by this. The wanted rate R_b of the communication system will then be limited by the available channel bandwidth

B and possible received power to noise:

$$R_b < C \Rightarrow \frac{T f_s f_p}{M} < B \log_2(1 + \frac{\bar{P}_r}{P_N}) \tag{3.1}$$

There are many factors that influence the coverage and range for a communication system [18]. Multipath or other attenuation factors will greatly influence the SNR at the receiver, but are excluded for the sake of simplicity. A link budget could be set up to find the range using an appropriate path-loss model, and a required SNR for the receiver. The coverage would also depend on the antenna used, as its aperture will determine where, in both azimuth and elevation, the signal is radiated. The BER P_e for a BPSK modulated DSSS system will depend on the received symbol energy E_s, in the presence of Gaussian noise from Equation 2.26. Even though the processing gain will be equal the spreading factor M, the total transmitted energy E_t is still the same when using BPSK and DSSS.

3.1.3 EW Performance

EW performance is in this thesis split into either EP or EA capabilities. EP is the waveforms ability to be undetected by a ES receiver, or LPI. One way is making sure the waveform is hidden below the noise floor of the ES receiver. The use of a noise-like waveform will have preferable LPI properties, as summarized by Pace [3]:

> " The use of noise waveforms can result in a large mismatch in processing gain between the radar and the noncooperative intercept receiver making their presence hard to detect."

However, a high-power noise waveform is still trivial to detect using ES equipment. Making the MW low powered and noise-like will enhance EP. EA capability will predominantly depend on the target receiver/system. Reducing capacity and BER will depend on the ability to increase JSR. The need of ES is important to set the correct carrier frequency and bandwidth. However, this thesis considers the transmission and detection of own waveforms, and not the ability to detect other signals.

3.2 Design Variables

The general design variables or *degrees of freedom* and how they affect the various RF functions are listed in Table 3.1. Note that when a variable is discussed, it is under the assumption that the others are fixed.

Table 3.1: Figures of merit, and how design variables affect them

Design Variable	**Radar**		**Communication**			**EW**		**System**
	Range	Resolution	Range	bit rate	BER	EP	EA	Battery
Pulse length	T_p	$\Delta f_d \propto T_p^-1$		T_p		T_p	$T_p > T_t$	T_p^{-1}
Transmit power	P_t		P_t	P_t	P_t	P_t^{-1}	P_t	P_t^{-1}
Bandwidth	B^{-1}	$\Delta R \propto B^{-1}$				B	$B \geq B_t$	
Wavelength	λ^2	$\Delta v_r \propto \lambda$	λ^2				$f_c \approx f_t$	
Spreading factor				M^{-1}	M	M		
Duty cycle	CPI	$\Delta f_{PD} \propto T_{PRI}^{-1}$		T_{PRI}^{-1}			\$T_{PRI}	

Pulse duration

T_p: A longer pulse will result in a higher PSR and affects the max radar range as the pulse contain more energy. It decreases Doppler tolerance, and/or increases Doppler resolution depending on the Doppler processing used. For a fixed PRI and spreading factor, a longer pulse will contain more data symbols increasing bit rate. It enhances EP as the transmitted power can be decreased. In a pulsed EA system T_p must be above the target communication system symbol time. A longer T_p put a higher demand on the receiver hardware, as the correlation duration T_{int} is longer.

Transmit power

P_t: A higher power improves both ranges R_{max} and R_c, increases the SNR at the receiver, as well as JSR at a potential target receiver. Transmitting with higher power degrades LPI characteristics and battery consumption (for a given transmit duration).

Bandwidth

B: Wider bandwidth gives a finer range resolution, and increase the channel capacity and potential bit rate, but will increase the noise at the receiver and is generally limited by the choice of hardware for digital systems. In an EA setting, a wider pulse bandwidth than the target bandwidth will not be beneficial, on the contrary one would need a higher transmit power to achieve the same jamming effect. A smaller bandwidth will, depend on the target system, need increased power to achieve the same effects as a

matching bandwidth [2].

Carrier frequency / Wavelength

$fc = c/\lambda$: Higher f_c would increase the Doppler resolution, but affects the radar range, as well as communication range due to Friis Equation 2.23. To function as a EA system, the carrier frequency must be close to the target carrier frequency

Spreading factor

M: Spreading enhances stealth performance, as it will spread symbol energy E_s over a wider bandwidth B compared to not spreading the signal. It will be possible to hide the signal in noise, as the processing gain will pick it up again on the receiver side. If the signal is affected by frequency-specific noise, interference, or jamming, the spread sequence can still be processed by the receiver. The spreading factor is therefore important for both the stealth performance and interference-/jamming -resistance. If the data is not random, M is also important to make the waveform noise-like to get the radar-characteristics of a noise radar. However, increasing spreading factor to achieve LPI will reduce the bit rate R_b.

Duty Cycle/PRF

f_p: Transmitting similar pulses will result in an unambiguous range, so lowering the duty cycle will increase that range. A duty cycle below 100 % will result in lower bit rates of the communication system, as well as a lower average BER at the target receiver in an EA setting. Higher PRF increases Doppler resolution if using pulse-Doppler processing.

Hardware specific parameters is not design variables in the same sense, but will also determine performance in a variety of ways. Processing power of the available SDR, power amplifiers and other RF components like antennas and DACs all limit the design choices in some way. A more powerful SDR may be able to process a longer pulse, and a longer CPI increase both processing gain and Doppler resolution. The power amplifier will limit the possible PAPR of the waveform, as it will behave non-linearly in those cases. Maximum sampling frequency f_s are usually adjustable, but limited in software defined systems. The sampling frequency available to the system will dictate the maximum available bandwidth, determine the pulse length when generating digital sampled waveforms and enable oversampling for better estimation of communication symbols. If the MRFS system is to be powered by batteries, the power consumption also play an important role. It will limit the maximum possible transmitted energy over time. This means the system must compromise between transmit power and available energy, if the MRFS link is to be operative over longer periods of time.

3.3 Waveform Design Tools

A waveform generator, analyzer and simulator have been made in MATLAB. The simulation flow graph is depicted in Figure 3.2. The generator produces waveforms with different design variables and spreading sequences presented in this chapter. Using the Communication System Toolbox of MATLAB [65], LFM-, phase coded- and noise-sequences are generated. They are in turn used as spreading sequences for BPSK modulated random data bits. Each of the waveforms can be processed in the waveform analyzer to provide information about theoretical performance, and find waveforms suited for different tasks. The analyzer uses the theoretical formulas, plots waveform characteristics, and check up against example performance criteria listed in section 3.1. The analyzer also performs simulations to estimate PSR. Finally, the waveforms have been tested in a simulator described section 3.5.

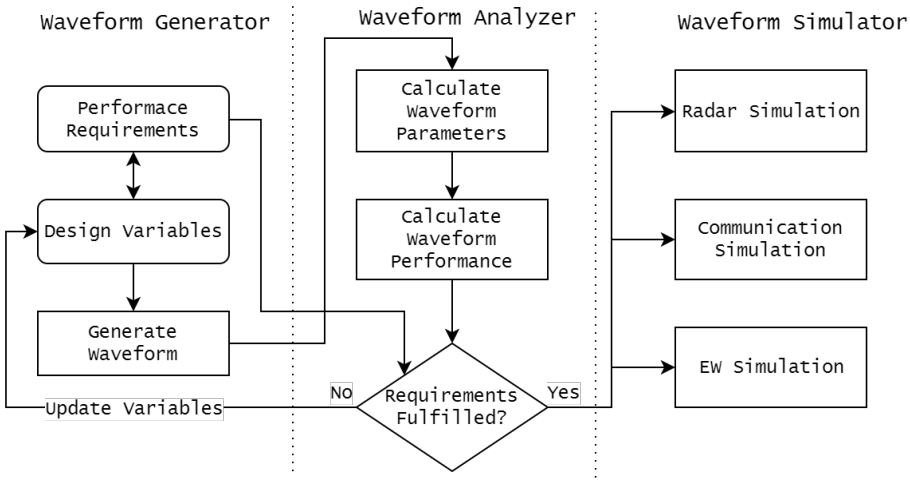

Figure 3.2: Flow diagram of the simulation

3.4 Multifunction Waveform Analysis

In addition to the design variables, the waveform modulation technique used as a basis for waveform generation is another degree of freedom. In this thesis the LFM, phase coded and noise radar waveforms are analyzed, omitting frequency hopping and multicarrier modulations. The modulated (radar) waveforms will function as the spreading code in a DSSS system. Analyzing the AF will indicate the waveforms MF response. The PSR is very important for radar performance as it represents the ability to process out a detection from the MF. Note that the PSR only gives an indication of sidelobes in the zero Doppler cut $\chi(t_d, 0)$, and sidelobes may be higher in other areas of the AF. High sidelobes may result in erroneous detection when having strong target returns, or masking of weaker targets returns in the presence of strong clutter. High PSR is also important for the communication system, as some parts of the waveform will be needed to perform synchronization with a preamble.

3.4.1 Spread Spectrum LFM

LFM is one of the best-known radar-waveforms, using the LFM for communication on the other hand is challenging. Spreading LFM waveforms as done in [30] will partially destroy the good Doppler tolerance properties of the LFM waveform, and introduce high sidelobes in both time and Doppler. In Figure 3.3 the sidelobes grow with an increasing number of data symbols directly spread onto the LFM waveform. The symbols used is BPSK, meaning only the phase of the LFM is changed periodically according to the spreading factor.

Figure 3.4 show the development in PSR for different lengths of LFM waveforms, with a constant bandwidth of 25 MHz. 1000 different realizations of data symbols are spread with the same LFM to give an average PSR value. As expected the PSR is higher for waveforms with a higher time-bandwidth product, but there is a clear decrease in PSR when the length-to-spreading factor is around $N/M \approx 2^6 - 2^7$.

The distinct development of PSR for different length spread spectrum LFM waveforms can be described by the effects depicted in Figure 3.5. In red are the base LFM waveform of length $N = 1024$. In blue spread LFM waveforms with increasing spreading factor M. The side lobe of the random phase shift is added to the sinc-shaped sidelobes of the LFM, creating spurious effects resulting in a low PSR.

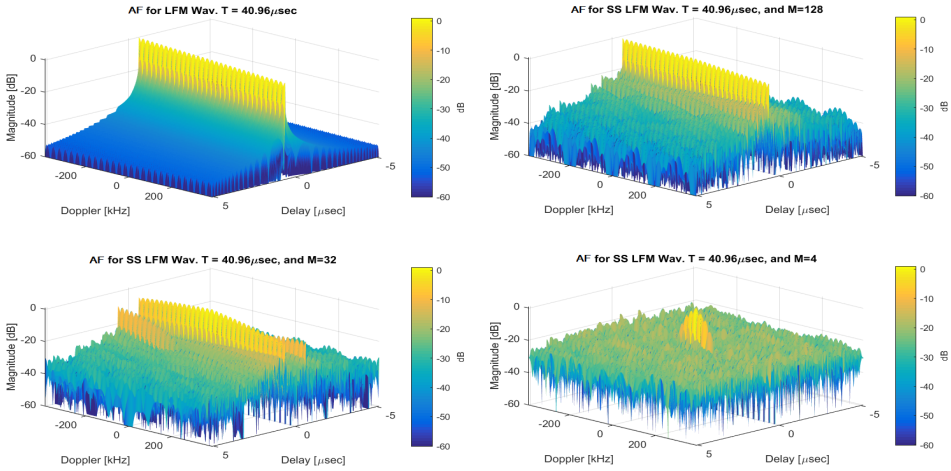

Figure 3.3: Spreading BPSK symbols onto a LFM radar waveform introduce sidelobes. Top left is the original waveform without any information. From the top right is spread spectrum (SS) LFM waveforms with $M = 128, 32, 4$ respectively

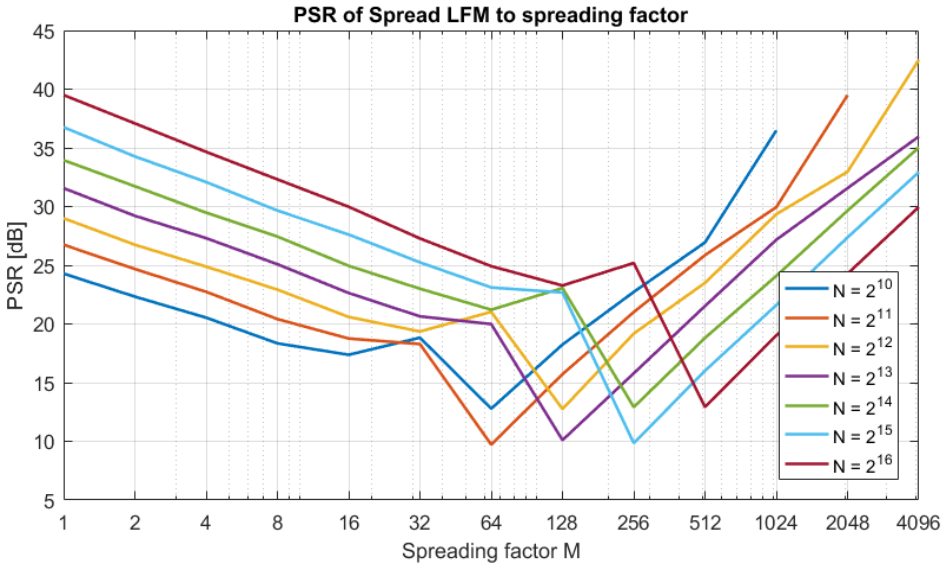

Figure 3.4: Different length spread spectrum LFM waveforms with increasing spreading factor.

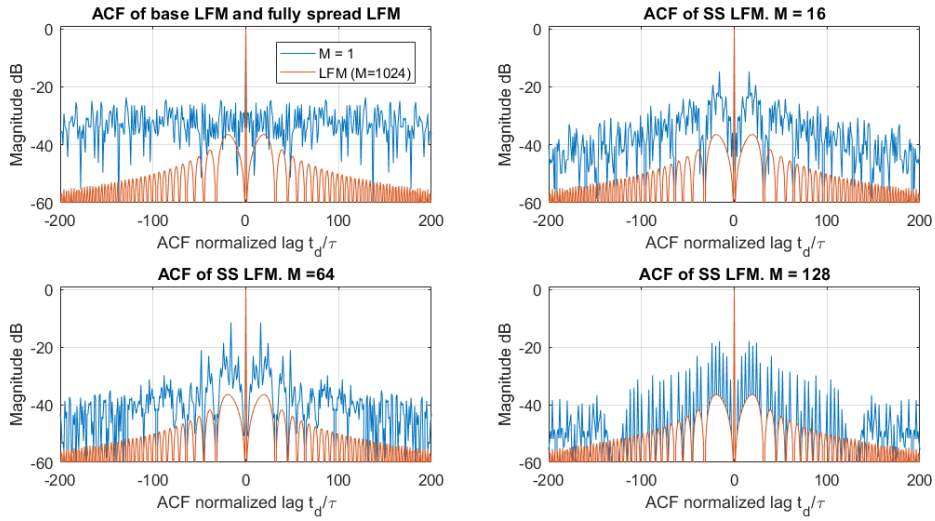

Figure 3.5: ACF for LFM as spreading sequence.

3.4.2 Phase Coded

Phase coded waveforms are known to both radar and communication systems. When designing an MRFS waveform using PSK it is important to look for good PSR in the codewords used, as it is directly linked to range and detection. Figure 3.6 compares the MF response of an arbitrary (MATLAB-generated) random-, ML-, gold, and Walsh-sequence of length $N = 2048$. Unmodulated Walsh-codes (purple) is not well suited for radar as its MF response have very high sidelobes due to its repetitive structure. Pure random BPSK coded bit-stream will have various PSR, but the sidelobes grows a bit higher than more optimized codewords. Gold codes (red) is optimized for cross-correlation, but its ACF is like that of random BPSK. ML codes has the highest PSR and will provide a good basis for MF optimized phase coded waveforms.

When information BPSK symbols are spread onto the ML code, it will break some of the good MF response. Figure 3.7 depicts the development with increasing spreading factor on different length ML codes. When the spreading factor is the same as the code-length (e.g. $M = N = 1024$), it represents the original ML code (either 180° phase-shifted or not), and the PSR increases significantly.

Simulation of the MF response comparing the short coding method (ML_s) and a long-code (ML_l and Rand_l) can be seen in Figure 3.8. The short code has a total length of $M = 32$, and repeated $L = 32$ times to form a sequence equal to the

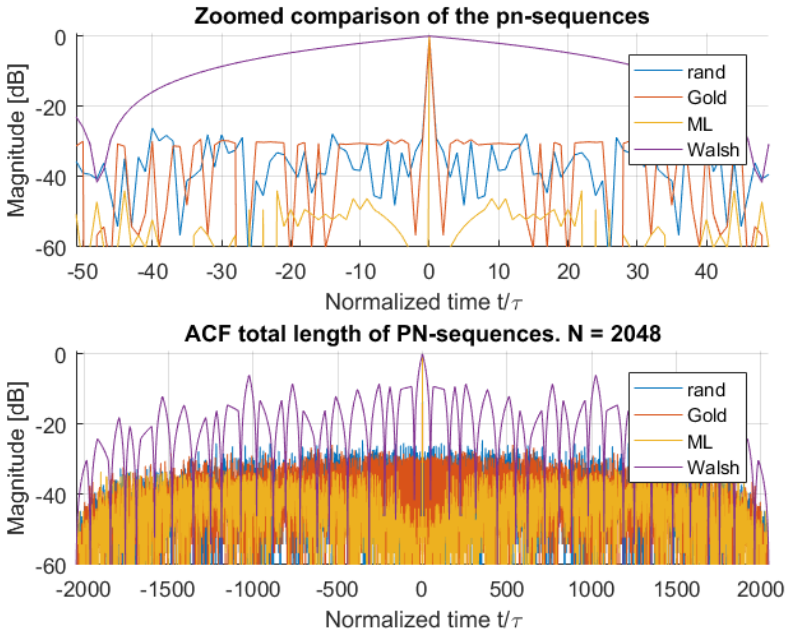

Figure 3.6: Comparing the ACF properties of rand-, ML-, gold-, and Walsh-sequences of equal length. N = 2048.

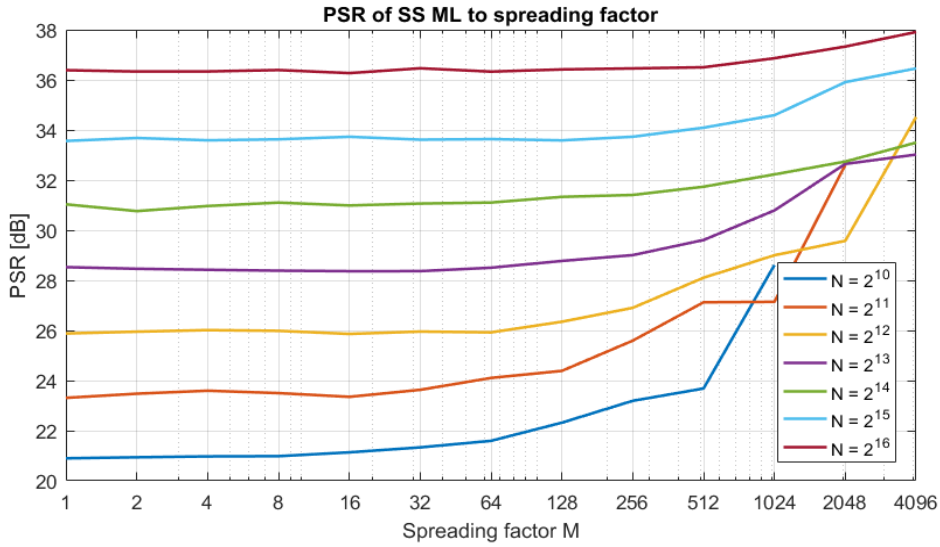

Figure 3.7: Different length ML code waveforms with increasing spreading factor.

long code of total length $N = 1024$. For the long coding technique both an ML sequence and a randomly generated BPSK sequence has been simulated. When no modulated symbols are present, the repeated short coding sequence will have poor PSR compared to an equal length long sequence as seen on top of Figure 3.8. The sequence is repeated several times, so the ACF shape for the short coding spreading sequence is expected. By using the sequences to spread BPSK symbols the PSR evens out a bit. However, there are still distinct sidelobe peaks by using the short coding technique depicted on the bottom of Figure 3.8. The PSR is the calculated mean from 1000 different information symbol constellations. The random sequence is also regenerated for each run, as some random sequences can have very poor ACF properties. When designing a sequence for matched filtering *given the bit rate and the sequence length*, it will be preferable to use long coding.

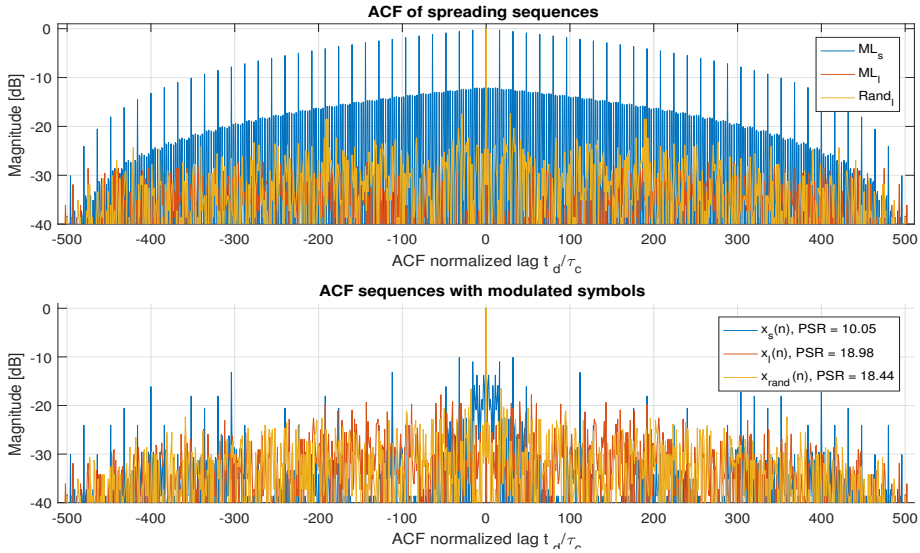

Figure 3.8: ACF of *short coding* and *long coding*. On top: ACF of a repeated ML short code, and a long ML and random BPSK sequence. Below: ACF of the spread sequences $x_s(n)$, $x_l(n)$ and $x_{rand}(n)$ using the above PN codes as spreading sequences

The bandwidth of bi-phase coded waveforms is given by the inverse of the chip duration for non-filtered chips. However, as the digital chips are sent via a DAC to RF components they are filtered in some manner. Bandwidth-dependent parameters like range resolution and EW-capabilities will therefore be highly dependent on the sampling-frequency of the software defined system the waveform is processed on. Digital filtering or oversampling of the chips will on the other hand improve communication capabilities. Synchronization-algorithms and eye-diagrams for the

communication receiver are more optimized when they can process on more samples.

The fast-changing pseudo-random phase of the BPSK modulated waveforms will result in a wideband and noise-like signal. The processing gain for both the radar and communication system will result in a potential for transmitting with low power, giving good EP. Increase the power, and the same waveform can be used as EA.

3.4.3 Noise

A pure noise waveform implemented in [66] would not be a *multifunctional waveform* in the same sense as the others discussed previously. However, by generating a digital pseudo-WGN sequence it can be used as a spreading code for information symbols. The waveform still possesses the complex WGN characteristics. The symbols can be processed out by a communication receiver that has the same spreading sequence. Figure 3.9 shows the PSR of BPSK symbols spread with a WGN sequence of length N. As the spreading sequence is already white, the added phase shifts of the information symbols will not change the PSR. The drawback with noise, is the demand for high complexity and resolution receivers. Each sample must be represented by an amplitude and phase, which each should come from a large library to achieve complex Gaussian noise characteristics. In MATLAB, 2×64 bits represent a complex sample.

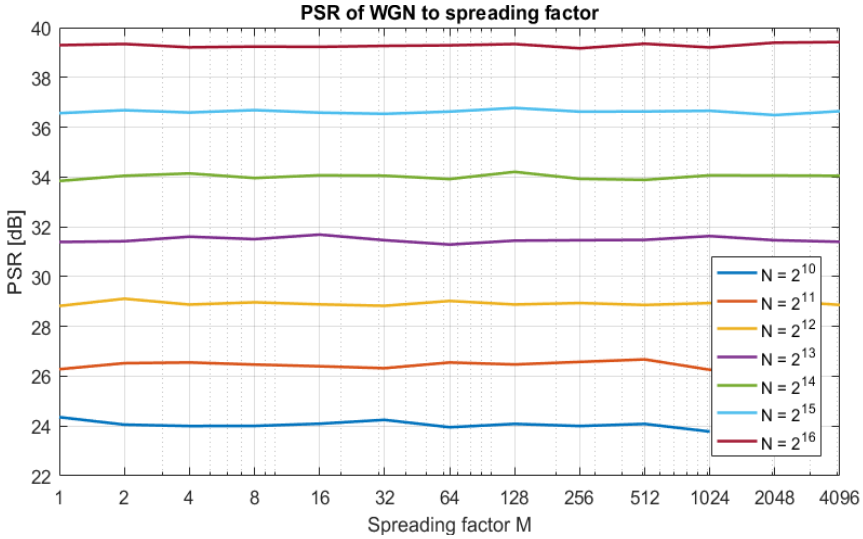

Figure 3.9: Different length WGN waveforms with increasing spreading factor.

3.4.4 Waveform Comparison

Figure 3.10 depicts simulations of the PSR of the different waveform modulation techniques used as spreading codes with a spreading factor of $M = 32$, and their non-information bearing equivalents. LFM would be the best waveform for a pure radar system. An LFM waveform of length $N = 1024$ has a PSR of 36 dB. Used with DSSS, the same length LFM modulated waveform has half PSR at 18 dB. For longer waveforms, the difference even increases. ML phase coded sequences also exhibit a reduction in PSR when spread, but the effect is only a reduction of approximately 20 % for the same spreading factor. ML by itself yields good radar performance, but quickly approaches random phase coded sequences as the BPSK information symbols destroy the original optimized ACF properties. WGN will not be affected by the information symbols, and has a higher PSR than just phase coded waveforms.

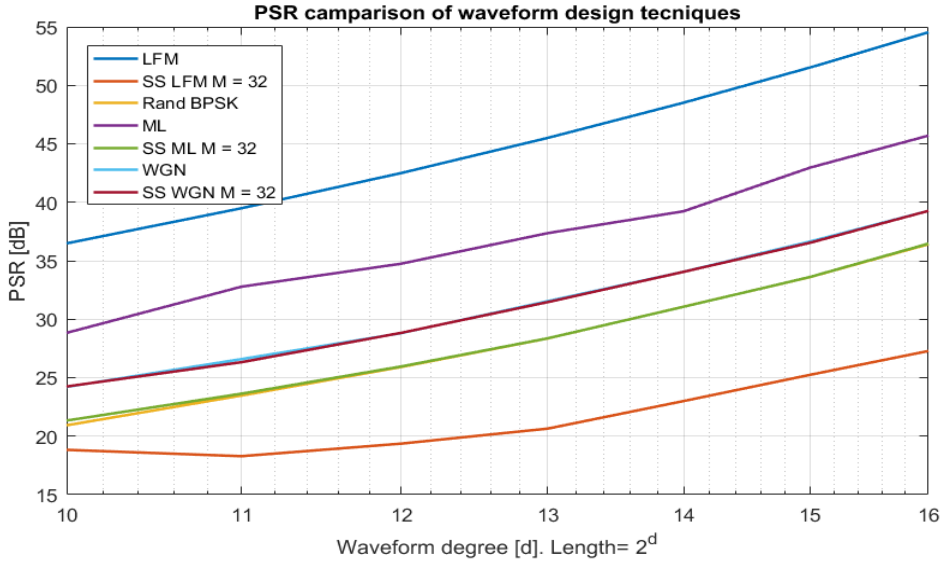

Figure 3.10: Comparison of different waveforms. The spreading factor for spread MWs are $M = 32$. At the x-axis is the degree [d] of the waveforms, where degree represents the length by $N = 2^{\mathrm{d}}$

Choosing a waveform modulation technique with respect to communication performance is dependent mostly on the energy per symbol E_S after synchronization is achieved. Synchronization is also dependent on high PSR, meaning both spread spectrum PSK and WGN is better suited as preamble than spread spectrum LFM. Both the LFM and PSK coded waveforms have constant amplitude, a very important feature for the amplifier hardware. The WGN coded waveforms would require

a more advanced power amplifier to handle the potentially high PAPR. A WGN waveform also introduces more complexity to the receiver as it will require more storage and more bits to achieve the proper resolution. The MF on a binary sequence will only require a phase and sign-comparator, as well as an initial phase and shift-register for storage and generation.

Bandwidth of the different design techniques are depicted in Figure 3.11. The simulated 99 % occupied bandwidth of the three methods is similar for a given sampling frequency. The sweep bandwidth of the LFM used as spreading sequence is equal to the sampling frequency of $f_s = 25$MHz. On the top right of Figure 3.11 is the spectrogram of the spread LFM. It shows that the instantaneous bandwidth is only wide whenever a phase shift occurs. This will affect the LPI properties of the waveform. The spectrogram of the phase coded- and WGN-waveform will be 25 MHz during the entire transmission time.

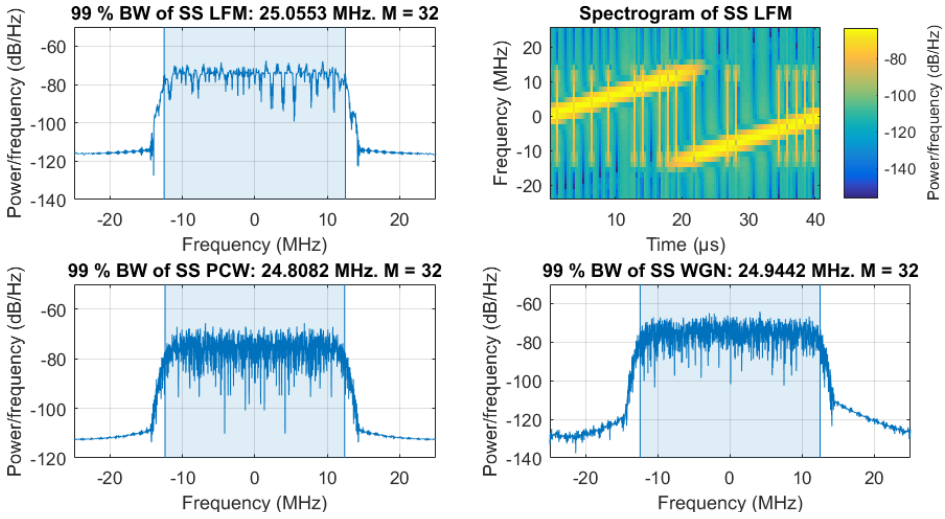

Figure 3.11: Overview of 99 % occupied bandwidth for the different design techniques. Top right is the spectrogram of the spread LFM waveform

3.5 Waveform Simulation

Waveforms are tested separately in the radar-, communication- and EW-simulators as depicted in Figure 3.2. The simulators are each created using the MATLAB Communication System Toolbox [65], and the radar simulator use objects from the Phased Array System Toolbox [67].

3.5.1 Radar Range Simulation

Radar simulations are performed as depicted in Figure 3.12. The first part of the simulation is the waveform generation described in section 3.3. Using a transmitter object, the waveform is amplified according to the given peak power P_t and transmit gain G_{tx}. The waveform is then free space attenuated, and reflected of a single point target. A simulated linear power amplifier will add noise to the received signal. Matched filtering is performed using the transmitted waveform according to Equation 2.10. As more pulses are transmitted they are stacked in a fast-, slow-time grid as shown in Figure 2.4. The MATLAB objects in the simulator had the values shown in Table 3.2.

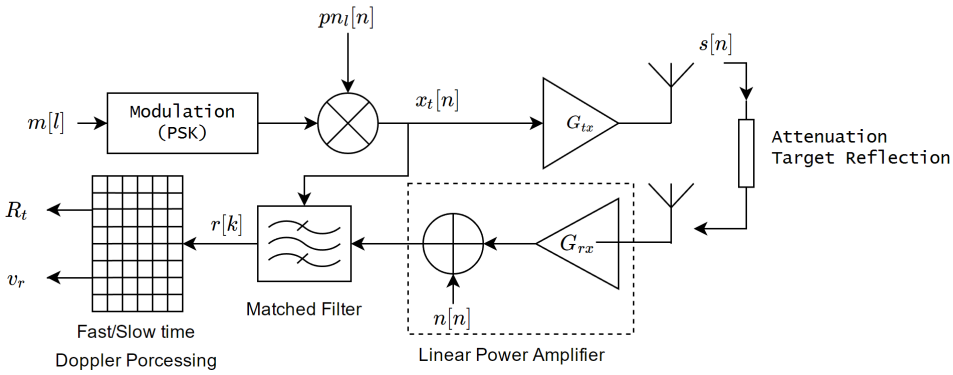

Figure 3.12: Block diagram of waveform generation, transmission, and radar receiver simulation

Each of the spread spectrum MWs analyzed in section 3.4 have been simulated and are depicted in Figure 3.13. The spread LFM waveform exhibits large sidelobes, and will even result in a false detection at approximately 1900 m. The MF response is also wide, reducing the range resolution. The phase coded and noise waveforms both show a distinct detection at approximately the target range. They also exhibit good range resolution, as the detection range is only represented by one sample in the fast-time grid.

Table 3.2: Values set for the Phased Array System Toolbox objects

Object	**Symbol**	**Value**
Transmitter gain	G_{tx}	40 dB
Peak power	P_t	1 W
Target RCS	σ	0.01 m^2
Target distance	R_t	1000 m
Receiver gain	G_{rx}	30 dB
Receiver noise figure	F_r	8 dB
MF length	T_{int}	T_p

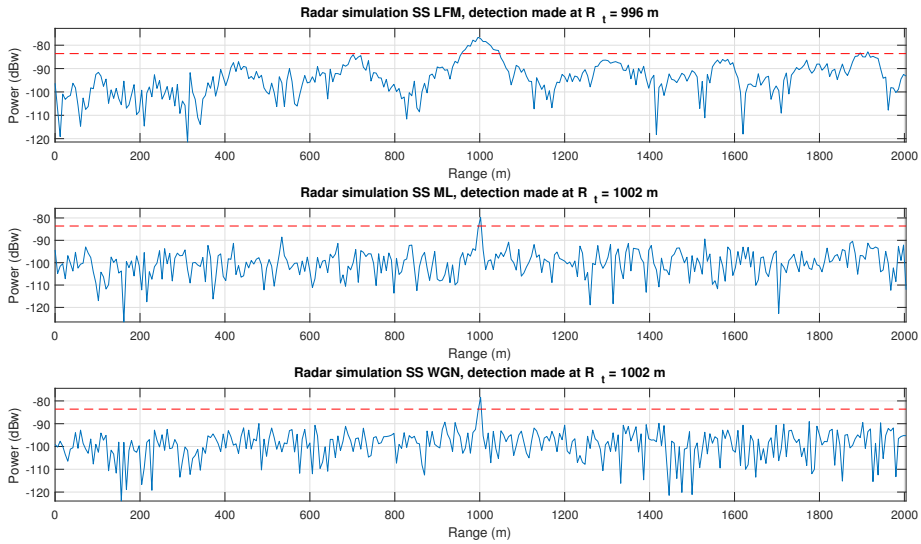

Figure 3.13: Fast-time and slow-time stacking of received radar pulses. From the top: LFM, phase coded and noise.

3.5.2 Communication BER Simulation

To estimate BER for the MWs from section 3.4 a communication simulator has been created. Each waveform is generated the same way as shown in Figure 3.13. The transmitted waveform is then added noise simulating an AWGN channel. The communication receiver is depicted in Figure 3.14. The received sequence is synchronous as discussed in section 3.4 and the filtering is performed in a chip synchronous system, with no oversampling. Each of the symbols are represented by M chips, M being the spreading factor. The M chips of symbol l are processed in a

matched filter taking the cross-correlation with M chips of the spreading sequence $pn_l[n]$. The peak of the cross-correlation is then demodulated using a *pskDemodulator* object [65]. BER estimation is then done by comparing the transmitted $m[n]$ and received $m_{est}[n]$ bit sequences.

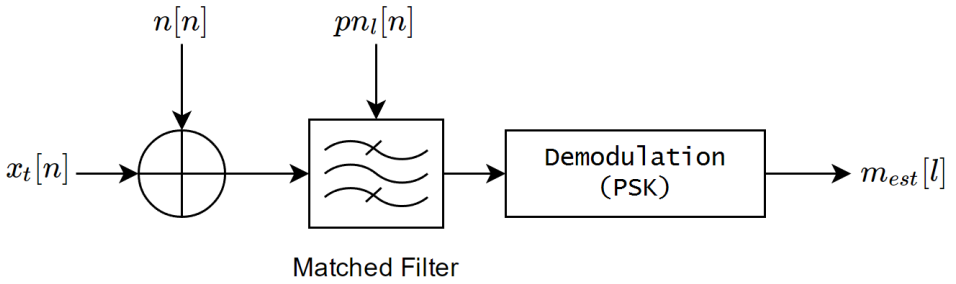

Figure 3.14: Communication receiver simulator.

The result of 50000 transmitted data sequences is depicted in Figure 3.15. Spreading factors simulated are $M = 1$, 4, 16 and 64. Each data sequence $m[n]$ contains $L = 32$ random bits. The AWGN channel and theoretical BER calculation were simulated using the chip SNR from Equation 2.28. On the x-axis is the chip-SNR. The blue dotted theoretical BER is calculated in MATLAB [65] as: berawgn($[E_c/N_0]_{dB} + 10\log(M)$). The LFM and ML spread simulations follow the theoretical BER calculations. However, data symbols spread by a WGN sequence provides a higher BER than the theoretical. Using noise as matched filter will lead to more errors than a phase coded or LFM spread sequence. In the case of a spreading factor of $M = 32$ and $E_c/N_0 = -10\,\text{dB} \Rightarrow E_s/N_0 = -10\,\text{dB} + 10\log(32) = -8.5\,\text{dB}$, WGN has a 22 % higher BER compared to theoretical. The additional error also increases with increasing SNR.

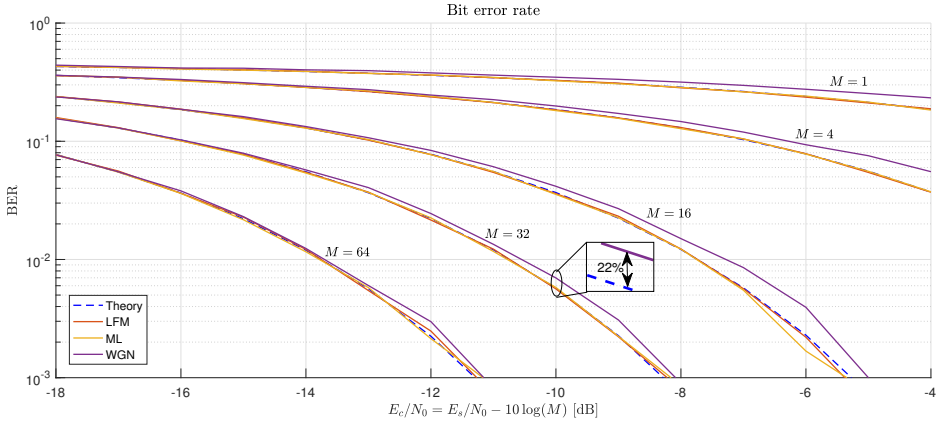

Figure 3.15: BER simulation using LFM, phase coded and noise spreading sequences. Spreading factors M are 1, 4, 16, 32 and 64.

3.5.3 EW simulation

To simulate EP capability, waveforms are processed in a non-cooperating ES receiver. A ES receiver could perform better with prior knowledge about the target signal. Many radars use LFM, so having a continuous LFM "matched"-filter would be a smart place to start. When transmitting a spread LFM, with SNR of 5 dB and $M = 32$, the left part of Figure 3.16 shows the potential output of a ES MF receiver. The ES receiver uses a detection threshold of 10 dB above the noise floor. The receiver also uses the exact LFM sequence used for spreading by the MRFS. Even a spread LFM waveform will give a detection response if the ES receiver matches on the frequencies and bandwidth used by the waveform. Fundamental structure in signals are easier to detect. The spread LFM has an underlying structure that can give enough processing gain in a non-cooperating receiver resulting in detection. On the right is a ES receiver trying to match with phase coded symbols. Both figures assume perfect timing on each chip/sample in addition to the prior knowledge about the transmitted waveform. In yellow is the MF response when using the same ML sequence as the DSSS communication system (ML). Even though there is an increase of signal power when the waveform is present, there is no clear peak as with LFM. For WGN, the effect is the same as for phase coded. There is an increase of power output from the MF due to the SNR of 5 dB. When using noise as MF the general noise level is slightly higher compared to phase coded. The ES receiver tries to match noise with noise, which in turn will not give any processing gain. Detection of noise, and phase coded waveforms, is possible when the waveform is above the noise floor of the ES receiver. Without perfect knowledge about both the spreading sequence *and* the information symbols the ES filter gives a low

response compared to having symbol match (blue). However, a multifunctional LFM waveform will give a detection where the phase coded are not.

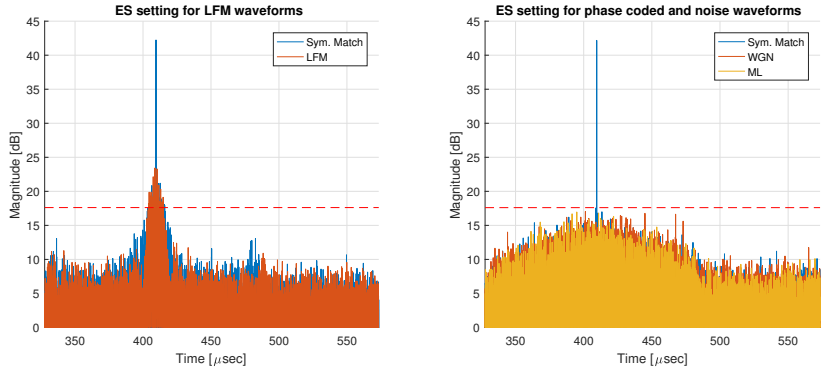

Figure 3.16: The filter response of a non-cooperating receiver trying to detect signal in noise. 0 dB represents the noise floor output of the matched filter. Left: LFM waveform, right: Phase coded waveform. SNR = 5 dB.

EA capability will be given by the JSR and the target communication system. Figure 3.17 depicts noise jamming of a BPSK communication link with SNR of 5, 10 and 15 dB. The simulation is performed by first adding the "normal" noise, then a jamming noise (J/S) with a given JSR. 10000 transmissions of information symbols in a random AWGN channel, with random WGN as interference was performed. Increasing JSR will result in more bit errors. The figure also shows that for high jamming power, the noise given by the SNR are neglected. With a JSR of 0 dB, a 5 dB SNR link will experience a BER of above 0.1. If a OFDM transmission uses BPSK, the transmission will begin to experience packet loss. A JSR of 15 dB will normally give a broken OFDM link as the BER is at 0.4. Note that error correction is not included in the discussion, for more on BER and OFDM see [59].

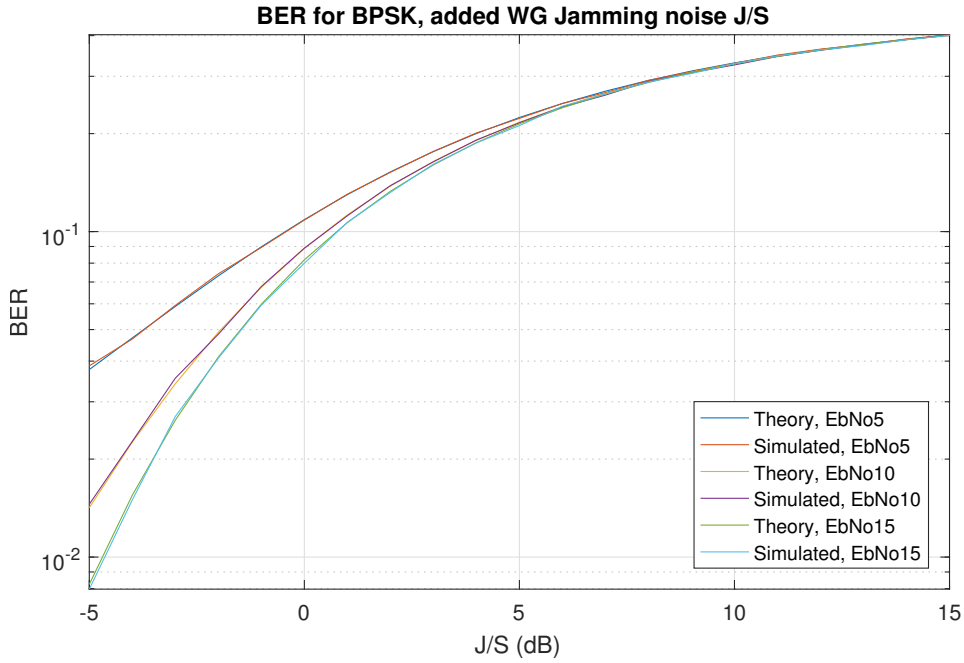

Figure 3.17: Theoretical and simulated BER for a BPSK communication link with SNR = 5, 10 and 15 dB.

Chapter 4

Areas of Application

In this chapter three area of applications are presented. The three scenarios each have distinct variations in required performance and functionality, but all based on the MRFS and MW design presented in this thesis. Note that these are all conceptual proposals for scenarios where an MRFS can be applied, and not directly tested or further analyzed in any form.

4.1 Scenario 1: LPI Search Radar and Ad-Hoc Navigational Beacon

The first scenario places the MRFS stationary on the ground as depicted in Figure 4.1. Functioning primarily as a search radar, covering a wide area of interest with its radar main-lobe. The radar-function has distinct LPI properties at first, transmitting with reduced power and in a limited bandwidth. The system is stationary and has a well-defined location. It can transmit that location in the waveform to friendly platforms within coverage. If it's known to the MRFS, it can also transmit the exact location of friendly platforms. Friendly platforms can include, but limited to; aerial drones, aircraft or ground-based navigation systems. In the presence of multiple ground-based MRFS the friendly platforms can use the navigation data to find its own position using techniques described in [68, 69].

The need for transmitting navigational data arises as enemy or unwanted platforms enter the area of interest. When the platform is detected and classified, the MRFS can switch to EA mode. It then tunes to an appropriate center frequency, placing the transmitted waveform over the assumed communication- and/or navigation-channel of the enemy platform. As the transmitted waveform is noise-like, by increasing the transmit power, it can disable the link. An example is disabling the Global Positioning System (GPS)-link. By doing so, friendly platforms will also loose GPS within the area of operation. The MRFS can now act as an ad-Hoc navigation beacon for friendlies, as it transmits its own location and/or the location of the other platforms. With increased signal power, there exist a possibility to increase data rate. The additional capacity can be used to transmit tracking data of objects in the scene or accurate positional data.

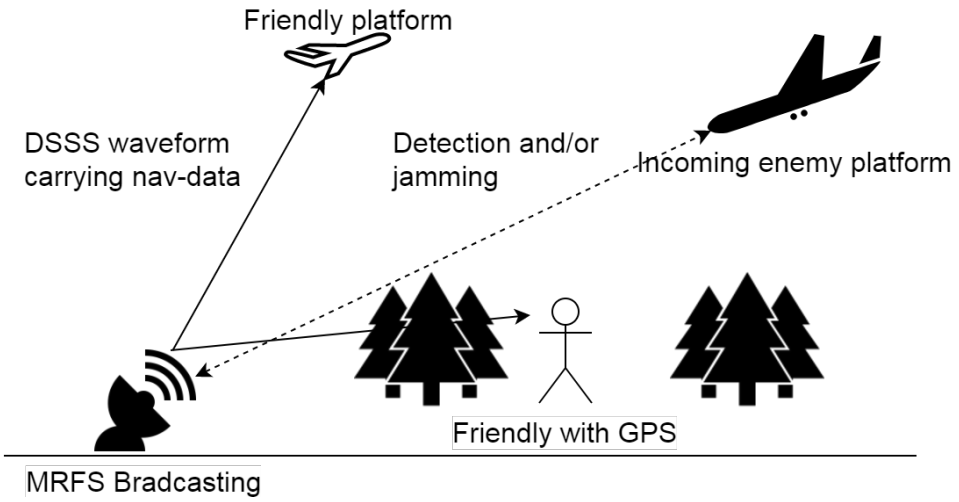

Figure 4.1: Sketch of Scenario 1: The MRFS first operating in search mode, with EA and navigational-beacon capability.

Important design variables would be bandwidth, transmit power and duty cycle. The waveform must also possess EW protection and attack capabilities. The bandwidth would need to cover the target communication link and provide a fine enough resolution to detect incoming drones. The transmit power must be low when in LPI mode, and potentially high when in EA mode. A constant duty cycle is needed to keep the communication link, as it will be the navigation data for friendlies in the area.

4.2 Scenario 2: RadCom SDR on a Drone

Cheap, small, and low power RadCom is the main idea in scenario 2. Shown in Figure 4.2 multiple drones are equipped with an SDR to perform aerial reconnaissance (radar) and internal communication. Placing RF equipment in the air will significantly increase potential range, as the free-space loss model of Equation 2.23 will be more valid. The drones can form an aerial ad-hoc network to communicate, and relay information as discussed in [70]. The coded communication signal could use CDMA to avoid interference within the network. CDMA also enables a netted radar system, as the coded signals reduce mutual radar interference. When a communication link is established between drones it enables signal cancelling [71]. This will further reduce interference. Detection of targets can be performed further away from the original location due to the network. When detection has been

made, the information is transferred back through the network to home base.

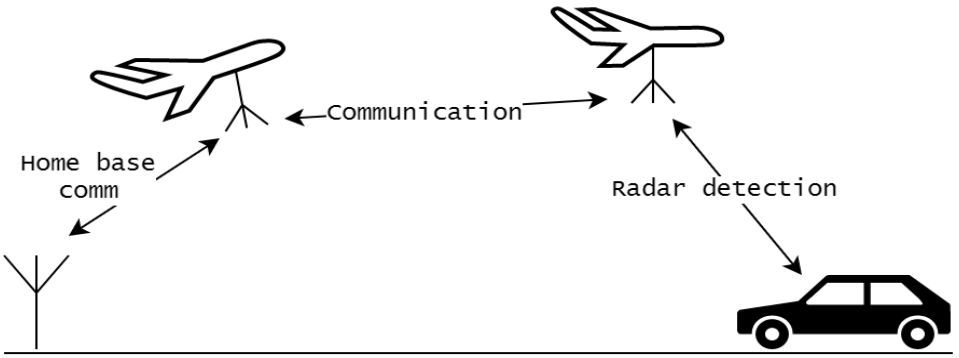

Figure 4.2: Sketch of Scenario 2: Drone implemented with a MRFS. Able to communicate and do radar detection at the same time.

Important design features for this design would be low power, pulsed signals with good EP properties. Orthogonal sequences, or sequences with good cross-correlation properties like Gold-codes are also important for a multiple user scenario. Battery capacity is limited for drones, so pulsed low power signals is key. A pulsed system would also enable the use of only one antenna.

4.3 Scenario 3: Convoy Communication and Jamming

A way of disabling radio controlled improvised explosive devices along roads is to set up a jamming "bubble" around the convoy [72]. This will disable communication between the controller and the explosive, but will also greatly limit the possibility to communicate within the convoy. If the jamming signal also contained information, the convoy coordinate without interference from a separate jammer. Without knowledge about the target communication-link, continuous barrage-jamming over a wide bandwidth is often the best approach. The convoy could also use the high-power jamming signal to do radar detection, as depicted in Figure 4.3. This would though require good isolation between transmit and receive antennas, and clutter removal as discussed by Malanowski and Kulpa [39].

A wide bandwidth, sufficient power and CW are fundamental features for such a scenario. The wide bandwidth must cover as much of the known communication links as possible. Frequency hops or sweeps is another solution, but must be performed quick enough to successfully jam potential transmissions [2]. The JSR

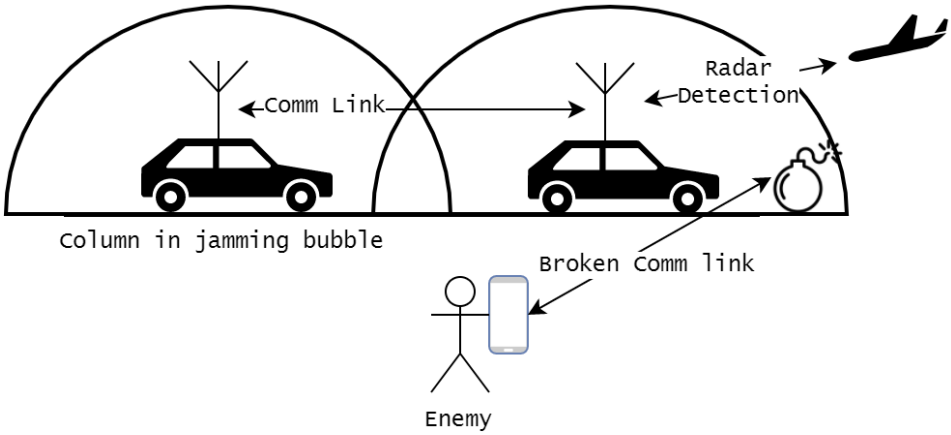

Figure 4.3: Sketch of Scenario 3: Convoy in a jamming bubble to break enemy communication link to potential IED, and perform radar detection.

must also be high enough for successful jamming leading to high power output. As discussed this put high demand on the power amplifier for linear operation, so a constant-amplitude signal is preferred.

Chapter 5

Multifunctional RF Demonstrator

A multifunctional RF demonstrator, based on scenario 1 in chapter 4, has been implemented and evaluated. Based on simulations discussed in chapter 3, MWs are designed and implemented on a COTS SDR system. The experiment was split up into sections (radar, communication, and EW) to partition the problem.

5.1 Waveform Design

To evaluate the MRFS of scenario 1 in chapter 4, an MW carrying information with sufficient EP and EA capabilities is required. It is also required to have search radar features. Example requirements for such a waveform are listed in Table 5.1. Detection of drones are discussed by Torvik et al. [73]. In the undertaken experiments, the RCS of the drones is approximated to that of a large bird at $0.01\,\mathrm{m}^2$. Typically, quad-copter drones have a maximum velocity of approximately $40\,\mathrm{m/s}$. Fixed-wing types may travel faster. Based on this the Doppler tolerance is estimated to ¿40 m/s. A range-resolution of maximum 10 meters allows the radar to detect incoming drones. At the same time, the radar has many pulses on target during the same range-cell to enable pulse integration. The radar function is also required to have a maximum, and unambiguous range above 500m. This will give at least 10 seconds of early warning. Thus, the waveform requires a specific length and PRF.

The bit rate of GPS is 1023 kbps [74], including both the data at 50 bps and code at 1023 kbps, is a good benchmark for scenario 1. This is because the waveform can be used to transmit navigation telegrams. To communicate with friendly platforms in the vicinity, a coverage of minimum 2 km is required.

The waveform should have good EP properties to avoid detection in low power mode. At the same time, the waveform should be noise-like and be sufficiently broadband to perform EA if required. Many civilian COTS drones normally use the IEEE 802.11 (Wi-Fi) standard. Communication includes telemetry and live video. The basic Wi-Fi standard in the 2.4 GHz is divided into 20-25 MHz wide

channels. Each channel use a bandwidth of 20-25 MHz for communication. The duration of each data symbol is 4 µs [75].

Table 5.1: Example Requirements

Prob. of Detection	P_d	0.9
Prob. of False Alarm	P_{fa}	10^{-4}
Range Resolution	ΔR	10 m
Doppler Tolerance	Δv	40 m/s
Doppler Resolution	Δv	5 m/s
Radar Range	R_{max}	500 m
RCS	σ	0.01 m^2
Bit Error Rate	P_e	10^{-5}
Bit rate	R_b	1023 kbps
Communication Range	R_c	2000 m
EA bandwidth	B_{EA}	20 MHz

The requirements listed in Table 5.1 are provided to the waveform analyzer MATLAB program. This determines design parameters listed in section 3.2, and waveforms which fulfill the requirements. For the multifunction experiments, the use of a DSSS ML phase coded and LFM modulated waveforms are further analyzed in this chapter. A waveform achieving the requirements is a DSSS waveform using an ML phase code with design parameters as listed in Table 5.2.

Table 5.2: Design parameters for the MW

Pulse duration	T_p	41 µs
Transmit power	P_t	1 W
Bandwidth	B	25 MHz
Carrier frequency	f_c	2.4 GHz
Spreading factor	M	16
Duty cycle	T_p/T_{PRI}	100%
Doppler processing	M_p	256

The waveform's AF, spectrogram and zero-cut's is depicted in Figure 5.1. The AF on top left has the sinc-shape in Doppler due to the finite integration time. The spectrogram on top right shows the waveforms wideband nature over the waveform duration. At the bottom left is the ACF having a PSR of approximately 20 dB, and the zero-time cut on the right shows a Doppler-tolerance of 24.4 kHz. Figure 5.2 shows an LFM waveform with the same design parameters listed in Table 5.2. From the spectrogram, it is shown that the phase coded waveform is better in terms of EP. This was also simulated in subsection 3.5.3. The phase coded waveform also has a higher PSR.

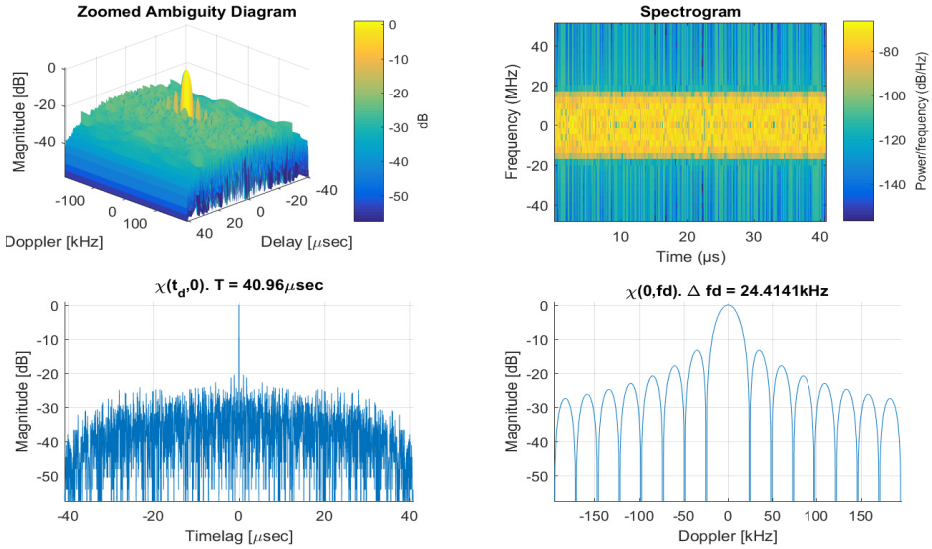

Figure 5.1: Analysis of a DSSS ML waveform.

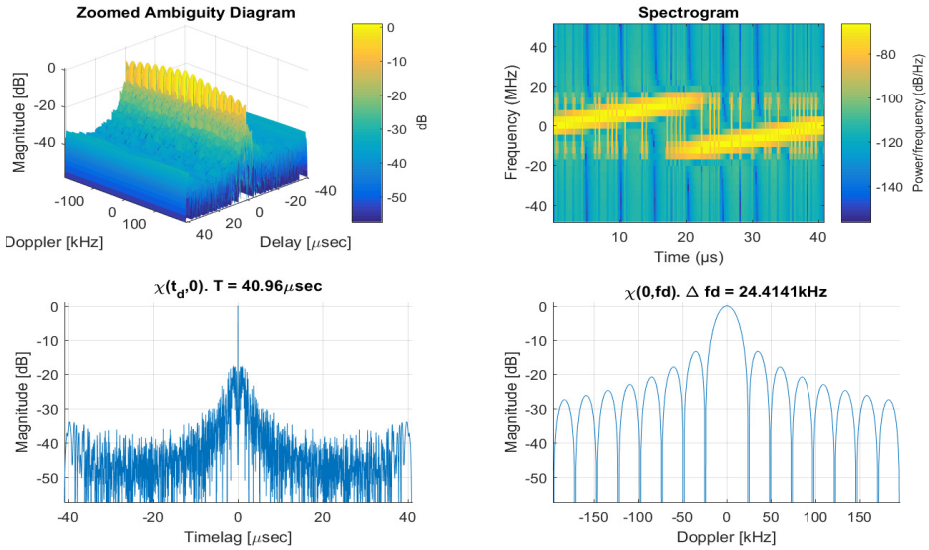

Figure 5.2: Analysis of a DSSS LFM waveform.

Calculations and simulations undertaken for the phase coded waveform are summarized in Table 5.3. For the radar range equations, a transmitter and receiver gain $G_{tx} = G_{rx} = 20\,\text{dB}$ are used. The communication range was calculated using the same transmitter, but with a 0 dB gain receiver.

Table 5.3: Theoretical calculations and simulation results

Radar range	R_{max}	820 m	from Equation 2.5
Unambiguous range	R_{un}	6.1 km	from Equation 2.1
Range resolution	ΔR	6.1 m	from Equation 2.14
Doppler tolerance	Δf_d	24.4 kHz	from Equation 2.22
Unambiguous velocity	v_{un}	371 m/s	from Equation 2.20
Doppler resolution	Δv_r	3 m/s	from Equation 2.19
Peak to side lobe ratio	PSR	20.5 dB	from Equation 2.11
Communication range	R_c	31 km	from Equation 2.30
Bit rate	R_b	1562 kbps	from Equation 2.31
BER	P_e	3.8×10^{-6}	from Equation 2.26

5.2 Waveform Verification and Implementation

The generated MWs are in turn implemented on a radar-, communication-, and EW-demonstrator. To demonstrate the capabilities of the same waveform for different RF functions gives more credibility to the software defined MRFS experiments.

5.2.1 Radar Demonstrator

To demonstrate the radar capabilities of the proposed MRFS an experiment was performed using the implemented USRP *cognitive radar testbed* by Christiansen et al. [43]. The equipment necessary to perform the experiment was already installed at the Norwegian Defence Research Establishment (FFI) site at Kjeller. Both hardware and software were implemented by Christensen. However, the waveforms evaluated were generated using the MATLAB tools presented in section 3.3. The hardware used was a National Instruments USRP-2952R [76]. The USRP-2952R has a powerful reprogrammable FPGA, and a maximum instantaneous bandwidth of 120 MHz. To achieve higher transmit power, a MiniCircuits ZVE-8G+ amplifier with a maximum of 10 W IP-3 was used together with the SDR. Horn antennas were used to achieve directionality, limit RF spill-over from Tx to Rx, and to provide extra antenna gain. The testbed, hardware, software, and RF components are presented in [43].

The experiment was installed on a rooftop as depicted in Figure 5.3. Pictures of the radar components and the target drone are shown in Figure 5.4. The target drone used was a 3D Robotics Solo Drone [77]. A dual-antenna radar setup enabled the evaluation of CW transmission. This is an important feature in the proposed system. The sampling frequency was set to $f_s = 25$MHz, similar to the simulation in section 3.5. The bandwidth corresponds to a OFDM Wi-Fi cell. However, in

the experiments, carrier frequency f_c was set to 3.15 GHz to avoid the interference within the 2.4 GHz band. This demonstrates the radar capabilities, and confirms to official RF regulations. The testbed implementation by Christensen is licensed to transmit at this frequency.

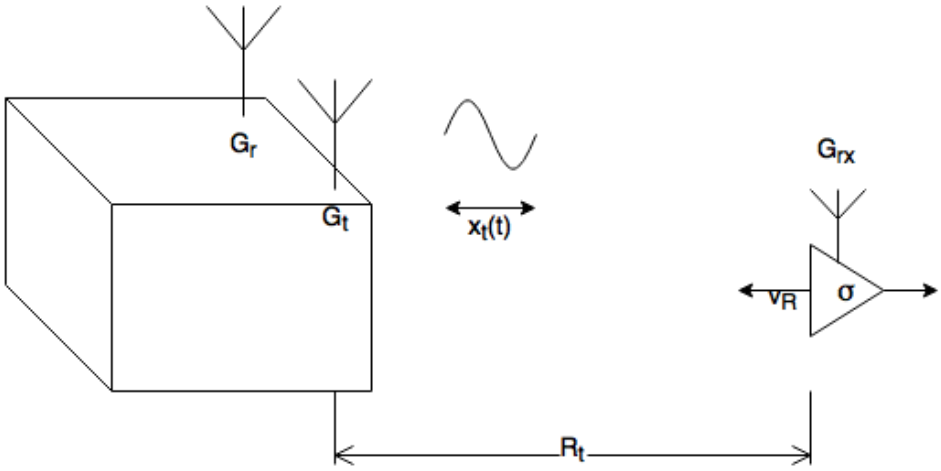

Figure 5.3: Schematic of the experiment undertaken.

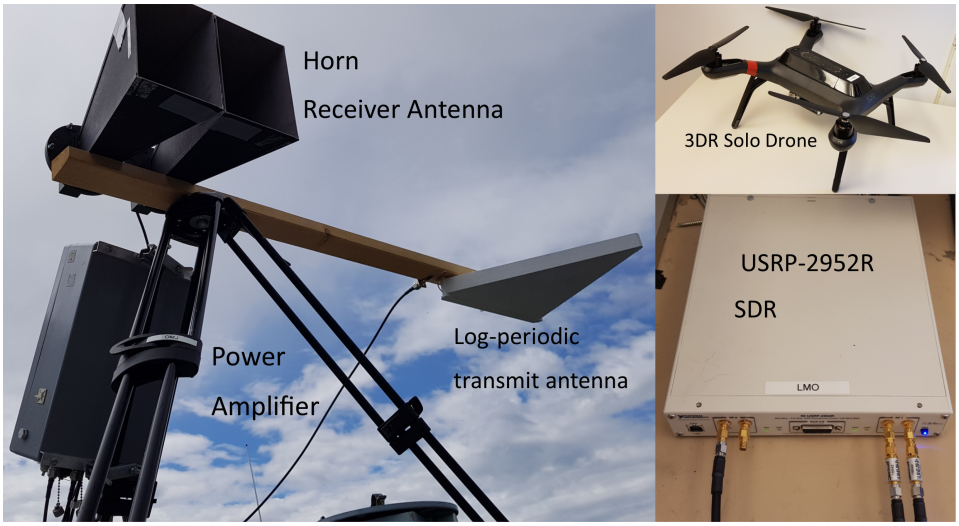

Figure 5.4: Pictures of the components in the radar demonstrator.

The detection of a drone with a phase coded MW is shown to the left in Figure 5.5. At a range of 71 m, travelling with a speed of 8.4 m/s, the drone was detected with a SNR of 20.25 dB. The noise level was calculated by taking the variance of samples in the outer edge of the Range-Doppler plot (far away, and high Doppler). The high SNR response in the zero Doppler range-cells was due to the local oscillator of the SDR. A local oscillator offset, and signal processing to remove clutter has the potential to improve detection. The high Doppler sidelobe response at approximately 10 m might be due to a large metal staircase close to the radar transmitter, and windy conditions.

The range-Doppler plot when a spread spectrum LFM waveform was used is depicted on the right in Figure 5.5. The high Doppler sidelobes made detection impossible. The figure is a snapshot showing one of the range-Doppler plots with the highest sidelobe interference. This was not observed all the time, but it was not possible to distinguish sidelobes from target returns. This demonstrates that spread LFM waveforms with the given design parameters are unsuitable for the radar function of a MRFS.

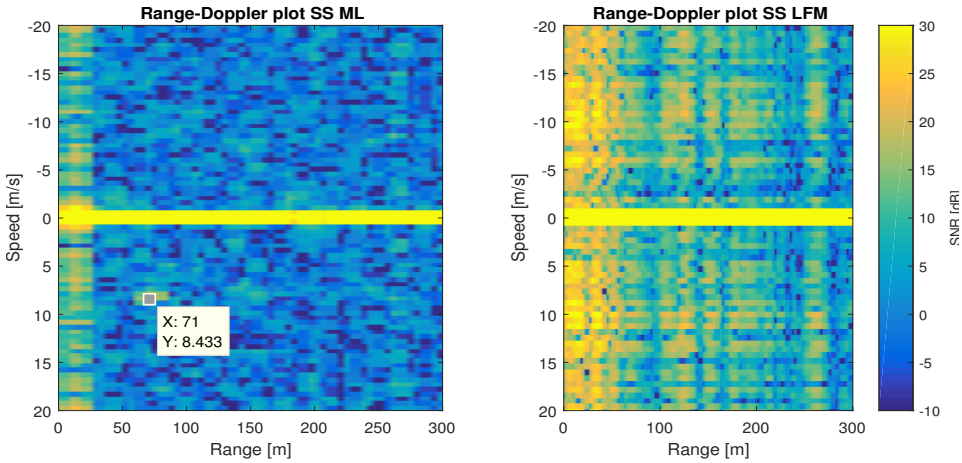

Figure 5.5: Range-Doppler radar plot of multifunctional waveforms. On the left: DSSS phase coded waveform. To the right: DSSS LFM waveform with significant sidelobes.

5.2.2 Communication

To demonstrate communication transmission, an Ettus Research USRP B210 SDR [42] was used to implement a communication transmitter. The B210 was used due to software and hardware availability. Before transmitting to a communication receiver, the waveforms were measured using a Rohde & Schwarz FSW spectrum analyzer [78]. This is to verify the bandwidth and power spectral density out of a COTS SDR. The phase coded waveform designed according to the parameters listed in Table 5.2 is depicted in Figure 5.6. The B210 SDR was used as a platform to transmit the waveforms. It was programmed using GNU Radio [79]. The waveforms were implemented in the B210 as complex samples, and not real-time generated as depicted in Figure 3.13. The bandwidth of the phase coded and noise waveforms is given by their chip rate, and should correspond to the bandwidth of a Wi-Fi channel. Hardware limitations in the setup prevents the B210 to transmit with a sampling frequency higher than 18 MHz.

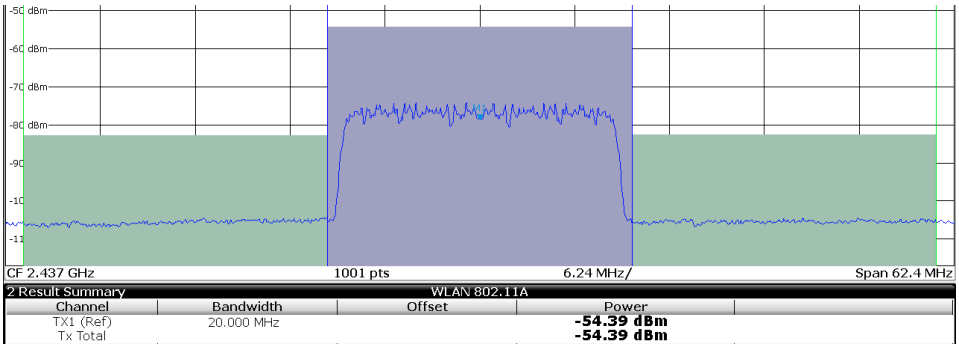

Figure 5.6: Screenshot on spectrum analyzer of the phase coded MW.

To demonstrate communication, the B210 was implemented as both transmitter and receiver via cable. The B210 has two Rx/Tx RF boards using the same local oscillator, enabling communication transmission without phase drift. The communication receiver was implemented as an ADC, directly storing complex samples in memory. The first synchronization stage was analyzed in MATLAB to verify that the symbols was transmitted correctly. Figure 5.7 shows the cross correlation between the received signal $y_r[n]$ and the transmitted signal $x_t[n]$. In this case, $x_t[n]$ is a data sequence with $L = 1024$ BPSK symbols spread with an ML sequence of length $N = 2^{15}$. This results in a spreading factor of $M = 32$. The upper figure shows the cross correlation with the entire sequence, resulting in a high PSR of 32 dB. In the figure below the MF knows only the first 8 data-symbols simulating a preamble of length $32 \times 8 = 256$. The resulting PSR was measured to be 7.6 dB. This is half of the theoretical processing gain of $10 \times \log(256) = 16.8$ dB.

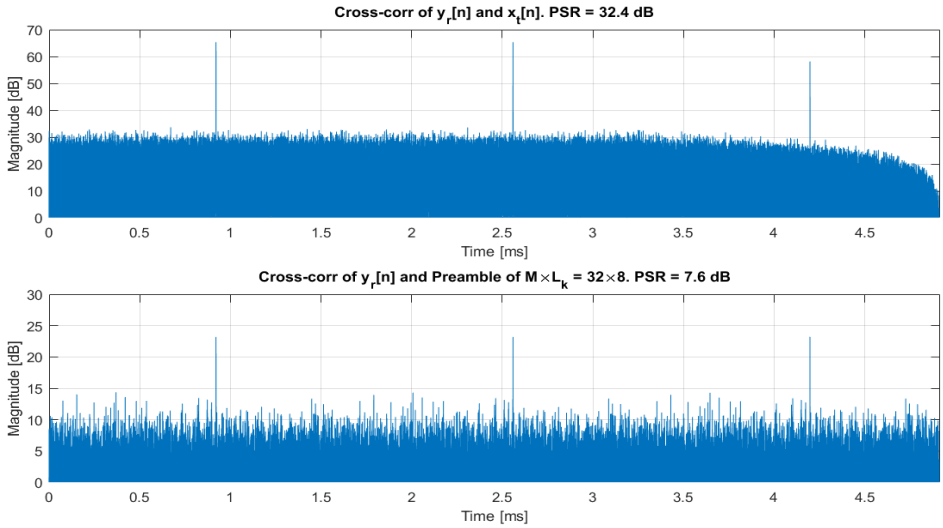

Figure 5.7: Communication synchronization experiments. On top the entire sequence is known. Below only 8 data symbols representing a preamble is known.

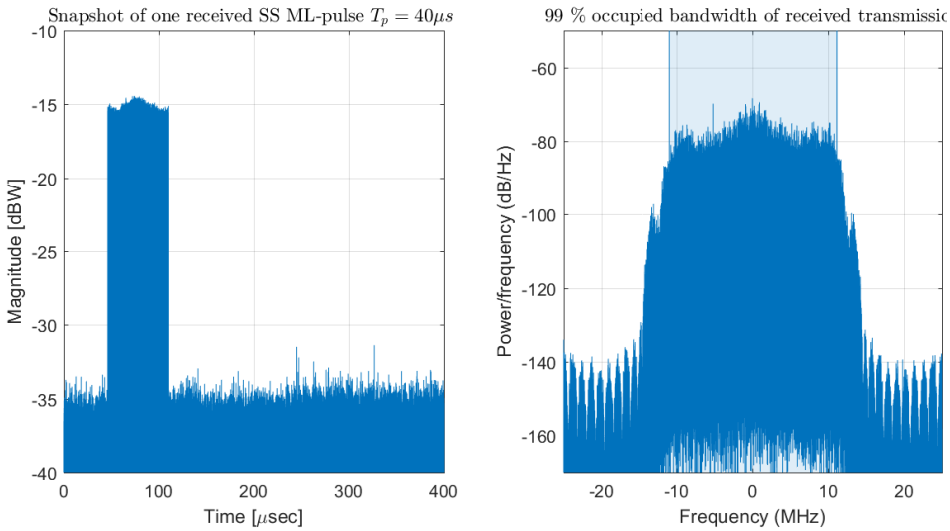

Figure 5.8: Reception of a MW on a B210 200 m from the transmitter. On the left is the time plot of the received pulse. To the right is the bandwidth plot.

Another more realistic communication experiment was undertaken. In this experiment, a B210 SDR was installed approximately $R_t = 200\,\text{m}$ away from the radar transmitter described in subsection 5.2.1. This is represented by the G_{rx}

antenna in Figure 5.3. The transmission was performed pulsed ($T_p < T_{PRI}$). The B210 was installed with a log-periodic antenna. The receiver SDR recorded data, and performed real-time spectrum analysis. The B210 used only a single receiver port. In this configuration, the SDR supports a sampling frequency of 25 MHz. The GNU-radio graphical user interface showed a significant increase of signal power around the correct carrier frequency during transmission. The recorded results are shown in Figure 5.8. On the left is the time plot showing an SNR of 23 dB. To the right is a bandwidth plot of the received sequence confirming the bandwidth of 25 MHz.

5.2.3 Jamming Capabilities

The EA transmitter was implemented the same way as the communication transmitter described in subsection 5.2.2. The designed waveforms have been assessed against a Wi-Fi link to analyze their capabilities as a jamming waveform. As a baseline, they are compared against complex wideband noise.

The experiment was performed as shown in Figure 5.9. Pictures of the system setup are depicted in Figure 5.10. An ASUS RT-N66U router [80] was configured using only one antenna port. The two other antenna ports were terminated. The router was configured to transmit packets of known data to a LogiLink Wi-Fi-dongle [81] on another computer. The iPerf measurement tool [82] was used on the receiver Linux computer to measure packet loss. Bit rate was approximated with the "iwconfig" command. 40 dB attenuation was inserted in the transmission path to simulate attenuation. Two RF splitters with a combined attenuation of ≈ 12 dB between the router and dongle enabled the insertion of the jammer signal and measurement with a spectrum analyzer. The top Figure 5.11 shows the bandwidth of the Wi-Fi transmission. The router was configured to transmit with a power of $P_t = 20\,\text{dBm}$. Within a bandwidth of 20 MHz (802.11 A) the receiver power is calculated to be $\bar{P}_r = 20\,\text{dBm} - 40\,\text{dB} - 12\,\text{dB} = -32\,\text{dBm}$. The measured power was -35.5 dBm. The Wi-Fi transmission in Figure 5.11 also shows the signal power is concentrated on each side of the carrier frequency of $f_c = 2.437\,\text{GHz}$. Measurement error correction was performed by measuring a sine wave from a Rohde & Schwartz SMIQ signal generator [83] on the spectrum analyzer. The error measured using the spectrum analyzer was consistently ≈ 3.5 dBm below the transmitted power. However, this did not affect the jamming results, as it is measured in JSR and packet loss.

The jamming signal is either Gaussian distributed wideband noise transmitted from a signal generator, or the MW from the B210 SDR. A variable attenuator is connected between the jammer and splitter enables control of JSR. The amount

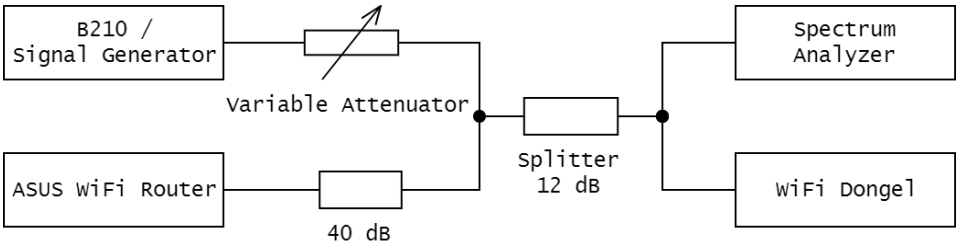

Figure 5.9: Block diagram of the jamming experiment

Figure 5.10: Pictures of the jamming experiment. Spectrum analyzer and signal generator are depicted on the left.

of packet loss with a given JSR does not give a valid BER estimation, but it gives an overall indication of jamming performance for the two techniques. Wi-Fi uses a carrier-sense multiple access protocol [84] with exponential backoff time. A Wi-Fi node measures received signal strength indicator (RSSI) before transmission. If RSSI is below a threshold, the Wi-Fi node will back off to avoid collisions. The result is that no transmission is performed when the RSSI is too low.

The wideband noise transmitted by the signal generator covers a bandwidth of 26 MHz. The blue line in the second picture of Figure 5.11 depicts the wideband jamming waveform at a JSR of 0 dB. The black line represents the integrated power after transmission. It shows the Wi-Fi power accumulated over the smaller symbol transmission bandwidth around the carrier frequency. Some packet loss was observed with JSR ranging from 0 to 10 dB. However, retransmissions at the same level showed no loss. Even with a significant reduction in bit rate, few errors were measured when JSR was further increased. A breakdown of the transmission was first observed with JSR = 13 dB. Further retransmission was possible until JSR of 20 dB. At JSR $>$ 20 dB, the experiments showed no further communication.

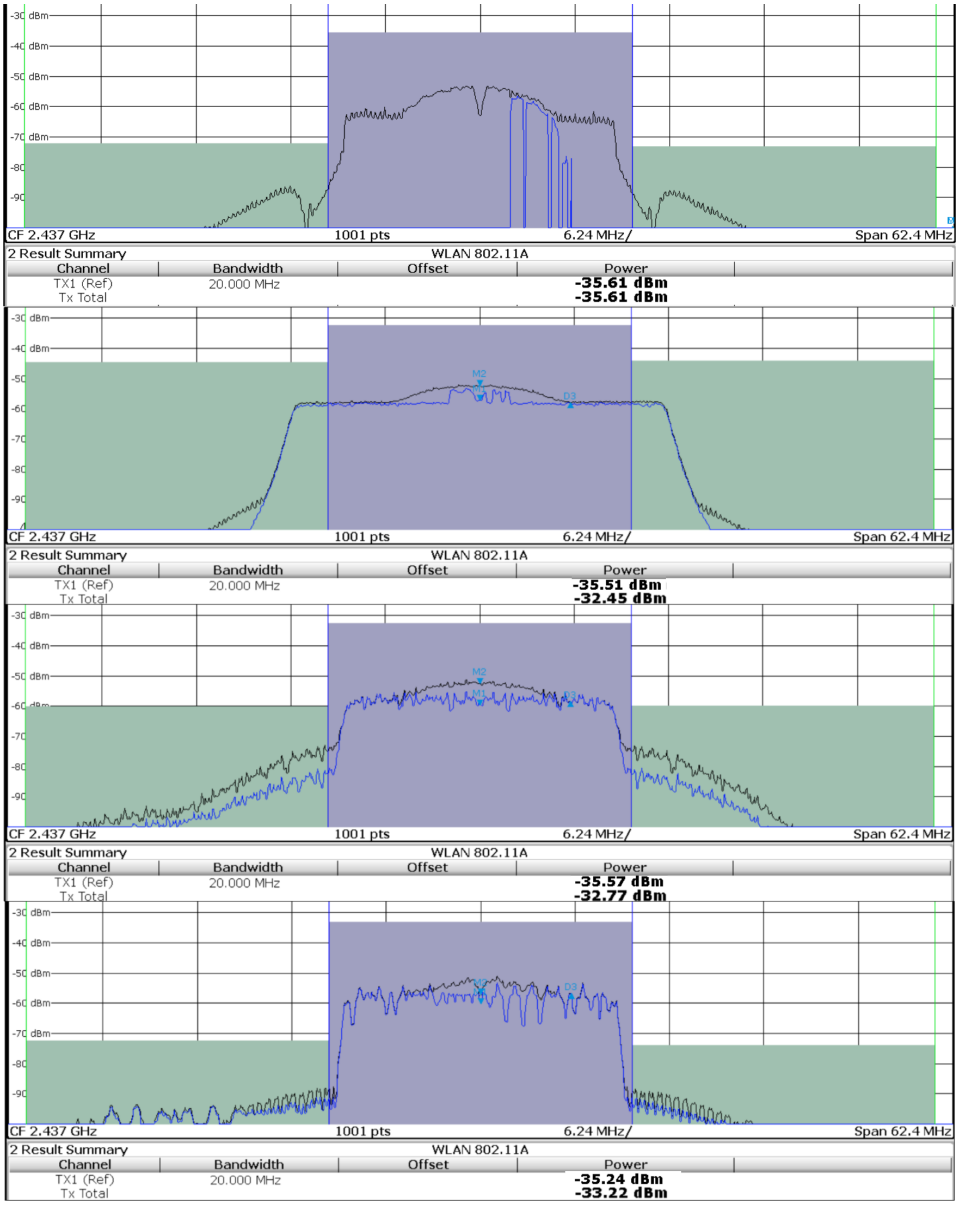

Figure 5.11: Spectrum of the Wi-Fi transmission and the three different jamming waveforms. From the top: Wi-Fi, Wideband noise 26 MHz, DSSS Phase Coded, DSSS LFM

The phase coded MW used as jamming signal was generated according to the specifications listed in Table 5.2. However, the maximum sampling frequency of

the B210 at f_s = 18MHz resulted in a reduction of the bandwidth as shown in Figure 5.6. With no Wi-Fi transmission, the transmitted power out of the SDR was measured to -35.57 dBm within the 20 MHz bandwidth. This was via the splitter and the variable attenuator set to 17 dB. This gave a JSR of approximately 0 dB. Errors was first observed at a JSR of 0 dB. A signal loss was observed at 3 dB. This is depicted in the third row of Figure 5.11. No transmission was performed at a JSR of 5 dB, and the connection was lost. With few retransmissions, the link was again established. Some packet errors occurred also with increasing JSR, but the link was first completely jammed at a JSR of 15 dB.

Spread spectrum LFM was also evaluated as a jamming signal in the experiments. Shown at the bottom of Figure 5.11, the spread LFM has a non-linear power spectral density. Within the 20 MHz the LFM was calibrated to a JSR of approximately 0 dB. Consistent packet errors were measured for a JSR of 0 dB. For a JSR of 3 dB the link was jammed, and no retransmission could be performed due to backoff.

Experimental results are listed in Table 5.4. Packet loss was observed for approximately similar JSR for the three waveforms. However, the experiments using a LFM modulated waveform successfully jammed the link at a lower JSR compared to the two other waveforms. It is possible that this is due to the shape of the LFM shown in the spectrogram in Figure 5.2. Wi-Fi is designed to handle interference, as it operates in the contested ISM environment. The LFM waveform puts high signal power at linearly increasing frequencies. Experiments with phase coded and noise waveforms showed difficulty jamming the link when the JSR was slowly increased. However, when switched on during transmission, both waveforms required significantly lower JSR of around 0 dB to jam the link. A non-constant jamming technique might be preferable when the targeting Wi-Fi.

Table 5.4: Experimental measurements

Jamming technique	**Bandwidth within 20 MHz**	**Packet loss J/S**	**Broken link J/S**
Wideband noise	20 MHz	3 dB	20 dB
Phase coded	18 MHz	2 dB	15 dB
LFM	18 MHz	-4 dB	3 dB

Chapter 6

Conclusion and Future Work

In this thesis, multifunctional RF systems and waveform design for an SDR have been analyzed and discussed. Information bearing waveforms have been implemented and simulated to compare performance metrics. Tools to generate, analyze and simulate waveforms were implemented to identify and assess the impact of design choices on performance. Experiments using LFM, phase coded and complex Gaussian noise as spreading sequences for binary PSK modulated data symbols were undertaken. Results show that direct spreading reduces dynamic range properties of LFM and phase coded radar waveforms. A spreading factor of 32 reduces the dynamic range of LFM waveforms longer than 1024 samples by a factor of > 2. For phase coded waveforms, the reduction is only around 20 %. Using the same spreading factor, and with SNR of 0 dB, simulations show noise waveforms have 22 % more bit errors compared to the two other modulation techniques. Simulations show that the EW protection properties of phase coded and noise waveforms are better than that of the LFM.

Implementation on an SDR to demonstrate radar-, communication-, and EW-capability in real world applications has been undertaken. Experiments with the implemented radar shows the capabilities of the software defined multifunctional system as a search radar. A small drone was detected with high SNR at a range of 71 m, traveling at a velocity of 8.4 m/s. The phase coded MW with a bandwidth of 25 MHz provides a range resolution of 6 m. In CW, the waveform also provides a bit rate of 1.5 Mbps. Experimental jamming results show that the waveform interfere and cause packet loss in a Wi-Fi communication link at a JSR of 2 dB. However, experiments show that an LFM modulated waveform is more efficient at jamming Wi-Fi. The results of simulated and demonstrated capabilities show the feasibility of implementing a multifunctional system on a COTS SDR.

6.1 Future Work

In this thesis, the performance criteria of the RF functions were analyzed separately. Implementing a fully functional MRFS on an SDR is a natural next step. The application areas presented provides inspiration to what multifunctional systems are capable of. The demonstrators implemented in this thesis was based on the first scenario described in chapter 4. They proved the feasibility of a multifunctional search radar implemented on a COTS SDR. The waveform generator can generate waveforms with adjustable parameters and modulated symbols. Implementing the generator on an SDR as depicted in Figure 3.13 allows for real-time operation. A communication receiver depicted in Figure 3.14 is implemented on other SDRs to receive and demodulate data symbols. However, real-time communication requires chip synchronization and symbol timing. Frequency calibration due to an oscillator offset in the two communicating SDRs is also required. For more on communication and channel estimation see [56, 57].

The short- and long-coding technique has been discussed with both ML and random BPSK phase codes. When the bit rate and the total sequence length is given, results indicate that long coding is the best choice. However, analysis of the effect of building a sequence of codewords with known good cross-correlation properties with the same short-coding technique would be interesting. Gold and Kasami sequences are such codewords. A given spreading factor generates different realizations of Gold sequences of the same length. These are in turn used to individually spread the modulated information symbols.

The analysis tools are implemented to support complex valued symbols. This means they can also analyze polyphase codes. Polyphase codes provide even better PSR than binary phase codes. This is because the phase (ϕ_k) can take multiple values. Polyphase codes are also more Doppler tolerant than binary codes and are discussed in detail in Pace [3, Chapter 5]. The expansion to higher order PSK symbol modulations enables better performance in terms of bit rate. However, BPSK is resistant to interference. This is an important feature to keep the BER low.

The chips discussed in this thesis are rectangular, but when sent to analog RF they are filtered. Digital filtering of the waveforms could potentially benefit communication receivers. Filtering of noise waveforms is discussed by Axelsson [38] and Malanowski and Kulpa [39]. Axelsson presents a method to further reduce the sidelobes of noise by filtering. Melanowski and Kulpa implement filtering for clutter removal. A raised cosine filtering function was implemented and is included in the waveform generator. However, the raised cosine filtered waveforms were not analyzed in this thesis. When filtered by an oversampling factor, the bandwidth of

the waveform is reduced. Due to limitation in sampling frequency, and the in the interest of covering the Wi-Fi bandwidth, research into filtering was discontinued.

The design parameter and modulation technique analysis presented in this thesis can be combined with multi-objective optimization methods. Pareto-optimal waveforms can then be found given a cost function derived from a given scenario. Moen [85] presents such multi-objective evolutionary algorithms for radar and radar jamming. The concept described in [85] can be developed to suit MRFSs discussed in this thesis.

A cognitive multifunctional system inspired by [43, 63, 64] adjust the design parameters presented in section 3.2 in real-time. By implementing a multi-objective optimization algorithm, the system finds waveforms capable to the current objective. Cognitive features like the adjustment of transmit power enable EW protection or attack capability as discussed in scenario 1. Adjustment of pulse length and bandwidth change the processing gain of the radar system. The cognitive MRFS is able optimize radar when the need for communication is low. The other way around, it can transmit at high bit rates, but at the cost of radar dynamics.

Bibliography

[1] J. Luddy. *The challenge and promise of network-centric warfare.* Lexington Institute, 2005.

[2] R. Poisel. *Modern communications jamming principles and techniques.* Artech House, second edition, 2011.

[3] P. E. Pace. *Detecting and classifying low probability of intercept radar.* Artech House, 2009.

[4] D. Erricolo, H. Griffiths, L. Teng, M. C. Wicks, and L. Lo Monte. On the spectrum sharing between radar and communication systems. In *2014 International Conference on Electromagnetics in Advanced Applications (ICEAA)*, pages 890–893, 2014.

[5] P. K. Hughes and J. Y. Choe. Overview of advanced multifunction RF system (AMRFS). In *Phased Array Systems and Technology, 2000. Proceedings. 2000 IEEE International Conference on*, pages 21–24, 2000.

[6] G. C. Tavik, C. L. Hilterbrick, J. B. Evins, J. J. Alter, J. G. Crnkovich, J. W. de Graaf, W. Habicht, G. P. Hrin, S. A. Lessin, D. C. Wu, and S. M. Hagewood. The advanced multifunction RF concept. *IEEE Transactions on Microwave Theory and Techniques*, 53(3):1009–1020, 2005.

[7] M. I. Skolnik. *Introduction to radar*, volume 3 of *Radar Handbook.* McGraw-Hill Education, 1962.

[8] J. Herd, D. Carlson, S. Duffy, M. Weber, G. Brigham, M. Rachlin, D. Cursio, C. Liss, and C. Weigand. Multifunction phased array radar (MPAR) for aircraft and weather surveillance. In *2010 IEEE Radar Conference*, pages 945–948. IEEE, 2010.

[9] J. A. Malas. F-22 radar development. In *Aerospace and Electronics Conference, 1997. NAECON 1997., Proceedings of the IEEE 1997 National*, volume 2, pages 831–839 vol.2, 1997.

[10] H. Frennberg, T. Boman, A. Ouacha, A. Nelander, B. Andersson, A. Eneroth, P. Grahn, L. Pääjärvi, M. Tulldahl, S. Ekestorm, P. Klum, T. Holmgren, and M. Alfredson. Simulation platform for multifunction RF-systems. concept description, design principles and development of v0.1. *FOI*, 2002.

[11] S. Quan, W. Qian, J. Guq, and V. Zhang. Radar-communication integration: An overview. In *The 7th IEEE/International Conference on Advanced Infocomm Technology*, pages 98–103, 2014.

[12] M. Otten, J. de Wit, F. Smits, W. van Rossum, and A. Huizing. Scalable multifunction RF system concepts for joint operations. In *Phased Array Systems and Technology (ARRAY), 2010 IEEE International Symposium on*, pages 492–497, 2010.

[13] N. Levanon. Classical radar waveform design. In *Waveform design and diversity for advanced radar systems*. Institution of engineering and technology London, 2012.

[14] C. Sturm and W. Wiesbeck. Waveform design and signal processing aspects for fusion of wireless communications and radar sensing. *Proceedings of the IEEE*, 99(7):1236–1259, 2011.

[15] M. Roberton and E. R. Brown. Integrated radar and communications based on chirped spread-spectrum techniques. In *Microwave Symposium Digest, 2003 IEEE MTT-S International*, volume 1, pages 611–614 vol.1, 2003.

[16] W. H. Fiden; D. W. Czubiak. Radar-telemetry system. In *US Patents*. United States Of America As Represented By The Secretary Of The Navy, 2007.

[17] S. D. Blunt and E. L. Mokole. Overview of radar waveform diversity. *IEEE Aerospace and Electronic Systems Magazine*, 31(11):2–42, 2016.

[18] T. S. Rappaport. *Wireless communications: principles and practice*, volume 2. Prentice Hall PTR New Jersey, 1996.

[19] N. Levanon. Multifrequency complementary phase-coded radar signal. *IEE Proceedings-Radar, Sonar and Navigation*, 147(6):276–284, 2000.

[20] Y. L. Sit, C. Sturm, and T. Zwick. Doppler estimation in an OFDM joint radar and communication system. In *2011 German Microwave Conference*, pages 1–4, 2011.

[21] J. R. Krier, M. C. Norko, J. T. Reed, R. J. Baxley, A. D. Lanterman, Ma Xiaoli, and J. R. Barry. Performance bounds for an OFDM-based joint radar and communications system. In *Military Communications Conference, MILCOM 2015 - 2015 IEEE*, pages 511–516, 2015.

[22] B. J. Donnet and I. D. Longstaff. Combining MIMO radar with OFDM communications. In *2006 European Radar Conference*, pages 37–40, 2006.

[23] J. Zhao, K. Huo, and X. Li. A chaos-based phase-coded OFDM signal for joint radar-communication systems. In *2014 12th International Conference on Signal Processing (ICSP)*, pages 1997–2002, 2014.

[24] N. Dinur and D. Wulich. Peak-to-average power ratio in high-order OFDM. *IEEE Transactions on Communications*, 49(6):1063–1072, 2001.

[25] S. C. Thompson and J. P. Stralka. Constant envelope OFDM for power-efficient radar and data communications. In *2009 International Waveform Diversity and Design Conference*, pages 291–295, 2009.

[26] T. C. Clancy. Efficient OFDM denial: Pilot jamming and pilot nulling. In *2011 IEEE International Conference on Communications (ICC)*, pages 1–5, 2011.

[27] R. R. Meyer and M. N. Newhouse. OFDM waveform feature suppression. In *MILCOM 2002. Proceedings*, volume 1, pages 582–586 vol.1, 2002.

[28] F. Liedtke, M. Tschauner, M. Adrat, and M. Antweiler. About electronic protection measures (EPM) for an OFDM wide band waveform. In *2013 Military Communications and Information Systems Conference*, pages 1–8, 2013.

[29] Y. Xie, R. Tao, and T. Wang. Method of waveform design for radar and communication integrated system based on CSS. In *Instrumentation, Measurement, Computer, Communication and Control, 2011 First International Conference on*, pages 737–739, 2011.

[30] X. Chen, X. Wang, S. Xu, and J. Zhang. A novel radar waveform compatible with communication. In *2011 International Conference on Computational Problem-Solving (ICCP)*, pages 177–181, 2011.

[31] Z. Zhao and D. Jiang. A novel integrated radar and communication waveform based on LFM signal. In *Electronics Information and Emergency Communication (ICEIEC), 2015 5th International Conference on*, pages 219–223, 2015.

[32] D. Gaglione, C. Clemente, C. V. Ilioudis, A. R. Persico, I. K. Proudler, and J. J. Soraghan. Fractional fourier based waveform for a joint radar-communication system. In *2016 IEEE Radar Conference (RadarConf)*, pages 1–6, 2016.

[33] D. Gaglione, C. Clemente, A. R. Persico, C. V. Ilioudis, I. K. Proudler, and J. J. Soraghan. Fractional fourier transform based co-radar waveform: Experimental validation. In *2016 Sensor Signal Processing for Defence (SSPD)*, pages 1–5, 2016.

[34] M. K. Simon, J. K. Omura, R. A. Scholtz, and B. K. Levitt. *Spread spectrum communications handbook*, volume 2. Citeseer, 1994.

[35] R. L. Pickholtz, L. B. Milstein, and D. L. Schilling. Spread spectrum for mobile communications. *IEEE Transactions on Vehicular Technology*, 40(2): 313–322, 1991.

[36] S. R. J. Axelsson. On the theory of noise doppler radar. In *Geoscience and Remote Sensing Symposium, 2000. Proceedings. IGARSS 2000. IEEE 2000 International*, volume 2, pages 856–860 vol.2, 2000.

[37] S. R. J. Axelsson. Noise radar for range/doppler processing and digital beamforming using binary ADC. In *Geoscience and Remote Sensing Symposium, 2001. IGARSS '01. IEEE 2001 International*, volume 5, pages 2001–2005 vol.5, 2001.

[38] S. R. J. Axelsson. Noise radar using random phase and frequency modulation. *IEEE Transactions on Geoscience and Remote Sensing*, 42(11):2370–2384, 2004.

[39] M. Malanowski and K. Kulpa. Detection of moving targets with continuous-wave noise radar: Theory and measurements. *IEEE Transactions on Geoscience and Remote Sensing*, 50(9):3502–3509, 2012.

[40] X. Shaojian, C. Bing, and Z. Ping. Radar-communication integration based on DSSS techniques. In *2006 8th international Conference on Signal Processing*, volume 4, page 1, 2006.

[41] S. J. Xu, Y. Chen, and P. Zhang. Integrated radar and communication based on DS-UWB. In *2006 3rd International Conference on Ultrawideband and Ultrashort Impulse Signals*, pages 142–144, 2006.

[42] Ettus Research. USRP B210 spec sheet. https://www.ettus.com/content/files/b200-b210_spec_sheet.pdf, 2017. Accessed: 2017-04-28.

[43] J. M. Christiansen, G. E. Smith, and K. E. Olsen. USRP based cognitive radar testbed. In *Proceedings of the IEEE RadarCon 2017*, Seattle, USA, 2017. IEEE.

[44] D. W. Tufts and A. J. Cann. On albersheim's detection equation. *IEEE Transactions on Aerospace and Electronic Systems*, AES-19(4):643–646, 1983.

[45] M. A. Richards, J. A. Scheer, W. A. Holm, et al. *Principles of modern radar*. Citeseer, 2010.

[46] F. Gini, A. De Maio, and L. Patton. *Waveform design and diversity for advanced radar systems*. Institution of engineering and technology London, 2012.

[47] P. M. Woodward. *Probability and Information Theory, with Applications to Radar*. Pergamon Press: Oxford, second edition, 1953.

[48] J. Xu, J. Yu, Y. N. Peng, and X. G. Xia. Radon-fourier transform for radar target detection, i: Generalized doppler filter bank. *IEEE Transactions on Aerospace and Electronic Systems*, 47(2):1186–1202, 2011.

[49] G. W. Stimson, H. D. Griffiths, C. J. Baker, and D Adamy. *Introduction to airborne radar*. SciTech Pub., third edition, 1998.

[50] R. H. Barker. Group synchronizing of binary digital systems, communications theory w. *Jackson (Ed.) Butterworth, London*, 1953.

[51] J. W. Franklin. Presentation on theme: Logo passive bistatic radar. Presentation downloaded des. 2016, Uploaded 2015.

[52] E. H. Dinan and B. Jabbari. Spreading codes for direct sequence CDMA and wideband CDMA cellular networks. *IEEE Communications Magazine*, 36(9): 48–54, 1998.

[53] B. M. Horton. Noise-modulated distance measuring systems. *Proceedings of the IRE*, 47(5):821–828, 1959.

[54] S. R. Saunders and A. Aragon-Zavala. *Antennas and propagation for wireless communication systems*. John Wiley & Sons Inc., second edition, 2007.

[55] J. A. Shaw. Radiometry and the Friis transmission equation. *American Journal of Physics*, 81(1):33–37, 2013.

[56] D. Tse and P. Viswanath. *Fundamentals of wireless communication*. Cambridge university press, 2005.

[57] U. Madhow. *Fundamentals of Digital Communication*. Cambridge University Press, 2008.

[58] S. Parkvall. Variability of user performance in cellular DS-CDMA-long versus short spreading sequences. *IEEE Transactions on Communications*, 48(7): 1178–1187, 2000.

[59] C. Shahriar, M. La Pan, M. Lichtman, T. C. Clancy, R. McGwier, R. Tandon, S. Sodagari, and J. H. Reed. Phy-layer resiliency in OFDM communications: A tutorial. *IEEE Communications Surveys & Tutorials*, 17(1):292–314, 2015.

[60] F. K. Jondral. Software-defined radio: basics and evolution to cognitive radio. *EURASIP journal on wireless communications and networking*, 2005(3):275–283, 2005.

[61] J. K. Holmes. *Coherent spread spectrum systems*. New York, Wiley-Interscience, 1982. 636 p., 1982.

[62] G. R. Tsouri and D. Wulich. Impact of linear power amplifier efficiency on capacity of OFDM systems with clipping. In *Electrical and Electronics Engineers in Israel, 2008. IEEEI 2008. IEEE 25th Convention of*, pages 134–136. IEEE, 2008.

[63] J. R. Guerci. Cognitive radar: A knowledge-aided fully adaptive approach. In *2010 IEEE Radar Conference*, pages 1365–1370, 2010.

[64] S. Haykin. Cognitive radar: a way of the future. *IEEE Signal Processing Magazine*, 23(1):30–40, 2006.

[65] MathWorks. Matlab: Communication system toolbox. https://www.mathworks.com/products/communications.html, 2017. Accessed: 2017-03-21.

[66] M. Meller. Some aspects of designing real-time digital correlators for noise radars. In *2010 IEEE Radar Conference*, pages 821–825, 2010.

[67] MathWorks. Matlab: Phased array system toolbox. https://se.mathworks.com/products/phased-array.html?s_tid=srchtitle, 2017. Accessed: 2017-04-10.

[68] T. S. Rappaport, J. H. Reed, and B. D. Woerner. Position location using wireless communications on highways of the future. *IEEE Communications Magazine*, 34(10):33–41, 1996.

[69] C. Woo Cheol, D. S. Ha, and D. Ni. Performance evaluation of an ultra wideband radiolocation system with directional beacon. In *Proceedings. 2004 IEEE Radio and Wireless Conference (IEEE Cat. No.04TH8746)*, pages 59–62, 2004.

[70] S. Rosati, K. Krużelecki, L. Traynard, and B. R. Mobile. Speed-aware routing for UAV ad-hoc networks. In *2013 IEEE Globecom Workshops (GC Wkshps)*, pages 1367–1373, 2013.

[71] C.P. Norman and C.R. Cahn. Strong signal cancellation to enhance processing of weak spread spectrum signal, 2001. URL https://www.google.com/patents/US6282231. US Patent 6,282,231.

[72] P. Mihelich. Jamming systems play secret role in iraq, 2007. URL http://edition.cnn.com/2007/TECH/08/13/cied.jamming.tech/index.html?_s=PM:TECH. Visited: 27.04.2017.

[73] B. Torvik, KE. Olsen, and H. Griffiths. Classification of birds and UAVs based on radar polarimetry. *IEEE Geoscience and Remote Sensing Letters*, 13(9): 1305–1309, 2016.

[74] GPS Navstar. Space segment/navigation user interfaces, interface control document gps (200). *ICD GPS*, 200, 2013.

[75] E. Perahia and R. Stacey. *Next generation wireless LANs: 802.11 n and 802.11 ac*. Cambridge university press, 2013.

[76] National Instruments. USRP-2952R datasheet. http://www.ni.com/datasheet/pdf/en/ds-538, 2017. Accessed: 2017-04-28.

[77] Inc 3D Robotics. Solo specs: Just the facts. https://3dr.com/blog/solo-specs-just-the-facts-14480cb55722/#, 2017. Accessed: 2017-06-25.

[78] Rohde & Schwartz. R&S FSW signal and spectrum analyzer product page. https://www.rohde-schwarz.com/us/product/fsw-productstartpage_63493-11793.html, 2017. Accessed: 2017-06-20.

[79] The GNU Radio Foundation Inc. Website about GNU radio. https://www.gnuradio.org/about/, 2017. Accessed: 2017-06-12.

[80] ASUSTec Computer Inc. RT-N66U data sheet. http://static.highspeedbackbone.net/pdf/Asus%20RT-N66U%20N900%20Gigabit%20Router%20Data%20Sheet.pdf, 2012. Accessed: 2017-04-28.

[81] 2direct GmbH. Logilink wireless LAN USB adapter. http://www.logilink.com/Products_LogiLink/Active_Network_Components/Wireless_LAN_USB_Adapter/Wireless_LAN_300_Mbit-s_USB_20_Micro_Adapter_WL0150.htm, 2014. Accessed: 2017-06-28.

[82] iPerf.fr. iPerf - the ultimate speed test tool for TCP, UDP and SCTP. https://iperf.fr/, unknown. Accessed: 2017-06-28.

[83] Rohde & Schwartz. R&S SMIQ signal generator product page. https://www.rohde-schwarz.com/us/product/smiq-productstartpage_63493-7561.html, 2017. Accessed: 2017-06-22.

[84] E. Ziouva and T. Antonakopoulos. CSMA/CA performance under high traffic conditions: throughput and delay analysis. *Computer communications*, 25(3): 313–321, 2002.

[85] HJ. F. Moen. *Optimizing software-defined radar and radar electronic warfare systems using evolutionary algorithms*. University of Oslo in co-operation with Akademika Publishing, 2013.